AEDC-TR-68-217

DEVELOPMENT OF DIAGNOSTIC METHODS FOR SEEDED AIR AND NITROGEN PLASMAS

H. N. Olsen, G. Bedjai, F. L. Kelly, et al.

Plasma Sciences Laboratories, Inc.
Van Nuys, California

December 1968

This document has been approved for public release and sale; its distribution is unlimited.

ARNOLD ENGINEERING DEVELOPMENT CENTER
AIR FORCE SYSTEMS COMMAND
ARNOLD AIR FORCE STATION, TENNESSEE

NOTICES

When U. S. Government drawings specifications, or other data are used for any purpose other than a definitely related Government procurement operation, the Government thereby incurs no responsibility nor any obligation whatsoever, and the fact that the Government may have formulated, furnished, or in any way supplied the said drawings, specifications, or other data, is not to be regarded by implication or otherwise, or in any manner licensing the holder or any other person or corporation, or conveying any rights or permission to manufacture, use, or sell any patented invention that may in any way be related thereto.

Qualified users may obtain copies of this report from the Defense Documentation Center.

References to named commercial products in this report are not to be considered in any sense as an endorsement of the product by the United States Air Force or the Government.

DEVELOPMENT OF DIAGNOSTIC METHODS FOR SEEDED AIR AND NITROGEN PLASMA

H. N. Olsen, G. Bedjai, F. L. Kelly, et al.
Plasma Sciences Laboratories, Inc.
Van Nuys, California

This document has been approved for public release and sale; its distribution is unlimited.

FOREWORD

The research reported herein was sponsored by the Arnold Engineering Development Center (AEDC), Air Force Systems Command (AFSC), under Program Element 6540215F, Project 4344, Task 434412.

The results of the research were obtained by Plasma Sciences Laboratories, Inc., Van Nuys, California under contract F40600-67-C-0017. The research was performed during the period from June 15, 1967 to June 15, 1968 and the manuscript was submitted for publication on July 15, 1968.

The reproducibles used in the reproduction of this report were supplied by the authors. Additional authors not shown on the report cover are L. L. Price and R. E. Martindill.

The investigation was conducted under the direction of Dr. H. N. Olsen, serving as Principal Investigator, with Mr. G. Bedjai assisting. The experimental work was carried out by a research team consisting of Mr. F. L. Kelly, Mr. R. E. Martindill and Mr. L. L. Price. The authors wish to acknowledge the assistance of M. Sullivan in the numerical processing of data and the preparation of the manuscript.

This technical report has been reviewed and is approved.

Vincent A. Rocco
2nd Lieutenant, USAF
Research Division
Directorate of Plans
and Technology

Edward R. Feicht
Colonel, USAF
Director of Plans
and Technology

ABSTRACT

Absolute emission coefficients of nitrogen atomic lines, of a wavelength increment of the $N_2^+(1-)(0,0)$ band system, of the electron continuum and of several atomic lines of the seed material have been measured in atmospheric pressure nitrogen and air plasma jets seeded with K_2CO_3 powder. Radial temperature distributions determined from measured emission coefficients have been compared as the mean temperature of the plasma was reduced from 6000°K to 3000°K. In the lower range, which is most characteristic of the AEDC seeded air accelerator, temperatures determined from both absolute and relative intensities of atomic lines of the seed material agree well with those obtained from the electron continuum. The best species of radiation for temperature measurements in the range of 2500°K to 4000°K has, as the result of this investigation, been selected to be the continuous radiation emitted by the seed material itself. Errors in temperature determined from the measured continuum and resulting from averaged variations in seed concentration and its uniformity of distribution are shown to be less than 5% in the lower temperature range.

TABLE OF CONTENTS

Section		Page
	ABSTRACT	iii
	LIST OF ILLUSTRATIONS	vi
	NOMENCLATURE	ix
I	INTRODUCTION	1
II	EXPERIMENTAL METHODS	2
	A. APPARATUS	2
	1. Plasma Jet	2
	2. Observation and Quench Chamber	3
	3. Seeding System	3
	4. Traversing Table and Calibration Arc	4
	5. Radiation Detection System	5
	B. INTENSITY MEASUREMENTS	5
	C. PLASMA JET OPERATING CHARACTERISTICS	6
III	ANALYTICAL METHODS	8
	A. SEEDED NITROGEN PLASMA COMPOSITION	8
	B. SEEDED AIR PLASMA COMPOSITION	12
	C. EMISSION COEFFICIENTS	15
	1. Atomic Nitrogen Lines	15
	2. Molecular Ion Band, λ 3914 $N_2^+(1-)(0,0)$	16
	3. Electron Continuum	17
	4. Atomic Potassium Lines	18
	D. TEMPERATURE DETERMINATION	21
IV	DISCUSSION OF RESULTS	23
V	CONCLUSIONS AND RECOMMENDATIONS	28
	REFERENCES	30

LIST OF ILLUSTRATIONS

Figure		Page
1	Schematic diagram of experimental apparatus	31
2	Photograph of arc apparatus shown schematically in Fig. 1	32
3	Photograph of spectrograph and recording apparatus shown schematically in Fig. 1	33
4	Schematic diagram of first plasma jet configuration	34
5	Schematic diagram of second plasma jet configuration	35
6	Schematic diagram of third plasma jet configuration	36
7	Schematic diagram of observation plenum chamber and quench chamber	37
8	Sample recorder traces of continuum intensity showing the stability of the unseeded jet (1), the pulsing nature of Metco feeder without the fluidizer (2), and the improvement resulting from the fluidizer (3), where the arrows indicate equivalent fluctuations	38
9	Schematic diagram of fluidizer used to improve the uniformity of seed distribution	39
10	Sample wavelength traces of the integrated intensity spectrum emitted along central ray of pure nitrogen jet of first configuration	40
11	Emission coefficient vs temperature for λ 7469NI, λ 4935NI and λ 3914 $N_2^+(1-)(0,0)$ band increment $\delta\lambda$ for unseeded 1 atm N_2 plasma	41
12	Emission coefficient vs temperature for λ 7469NI, λ 4935NI and λ 3914 $N_2^+(1-)(0,0)$ band increment $\delta\lambda$ for unseeded 1 atm air plasma	42
13	Observed structure of $N_2^+(1-)(0,0)$ band system in region of band head. Numbers in parenthesis refer to upper K' quantum numbers	43

Figure		Page
14	Emission coefficient of $\delta\lambda$ increment of $N_2^+(1-)(0,0)$ band system vs temperature for 1 atm nitrogen plasma with different seed ratios	44
15	Emission coefficient of $\delta\lambda$ increment of $N_2^+(1-)(0,0)$ band system vs temperature for 1 atm air plasma with different seed ratios	45
16	Emission coefficient of continuum vs temperature for 1 atm nitrogen plasma at different seed ratios. The same curves apply also to the 1 atm air plasma	46
17	Emission coefficient of λ 4871 KI line vs temperature for the 1 atm seeded air or nitrogen plasmas for different seed ratios	47
18	Emission coefficients of λ 4965 KI line vs temperature for the 1 atm seeded air or nitrogen plasmas for different seed ratios	49
19	Emission coefficients of λ 5832 KI line vs temperature for the 1 atm seeded air or nitrogen plasmas for different seed ratios	51
20	Emission coefficients of λ 6939 KI line vs temperature for the 1 atm seeded air or nitrogen plasmas for different seed ratios	53
21	An illustration of the graphical method used to obtain T(r) from the measured $\epsilon(r)$ and computed $\epsilon(T)$ for the $\delta\lambda$ increment of the λ 3914 $N_2^+(1-)(0,0)$ band for the 1 atm unseeded nitrogen plasma	55
22	Temperature dependence of the ratio of emission coefficients for the quartet groupings of rotational components of the $N_2^+(1-)(0,0)$ band system located at the wavelengths of the R branch components having K'=2 and K'=70	56

Figure		Page
23	Comparison of radial temperature profiles determined from various species of radiation emitted by the 1 atm pure nitrogen jet of the second configuration	57
24	Radial temperature profiles of the 1 atm seeded air plasma at two seed ratios	58
25	Radial temperature profiles of the 1 atm 0.88% seeded air plasma obtained from absolute emission coefficients of five different species of radiation	59
26	Radial temperature profiles of the 1 atm 0.94% seeded air plasma obtained from absolute emission coefficients of four different species of radiation as well as from the ratio of coefficients of two spectral lines	60
27	Radial temperature profiles of the 1 atm 0.76% seeded air plasma obtained from absolute emission coefficients of four species of radiation	61

TABLES

Table		Page
I	Operating characteristics and average internal properties of seeded and unseeded experimental plasma jets	62
II	Partition functions of species of particles included in plasma composition calculations	65
III	Computed number densities of the 1 atm K_2CO_3 seeded nitrogen plasma	66
IV	Computed number densities of the 1 atm K_2CO_3 seeded air plasma	68
V	Identifying parameters for doublet and triplet multiplets of the potassium atom	71
VI	Average energy levels, statistical weights and wavelengths for multiplets of the potassium atom	72
VII	Computed parameters for multiplets of the potassium atom	72

NOMENCLATURE

a	Volume ratio of seed to total gas
A	Transition probability, sec^{-1}
b	Mass ratio of seed to total gas
B_0	Rotational constant for N_2^+ molecule, °K
$\beta_{K'}$	Symmetry factor for N_2^+ ion
c	Velocity of light, cm/sec
C	Normalizing constant
E_e	Electronic state energy of N_2^+ molecule, °K
E_m	Upper excited state of atoms, °K
ϵ	Emission coefficient, watt/(cm^3-sr) or watt/(cm^3-sr-sec^{-1})
g	Electronic state statistical weight
K'	Upper rotational state quantum number
K''	Lower rotational state quantum number
λ	Wavelength, Å
$\delta\lambda$	Wavelength increment in region of $N_2^+(1-)(0,0)$ band head, Å
$\Delta\lambda$	Spectrograph effective slit function, Å
M_K	Molecular weight of potassium
M_{N_2}	Molecular weight of nitrogen
N	Number density, cm^{-3}
P	Total pressure, atm
P_i	Partial pressure of ith species of particles, atm
P_e	Electron partial pressure, atm
$q_{v'v''}$	Franck-Condon factor
$\bar{R}_e$	Average electronic moment
S_i	Equilibrium constant of ith species or relative line strength
T	Temperature, °K
X	Lateral position (horizontal coordinate)
Y	Spectral intensity (vertical coordinate)
Z_i	Partition function of ith species
Zeff	Effective charge of retarding ions

I. INTRODUCTION

The purpose of this investigation was to establish diagnostic methods for measuring temperature distributions within atmospheric pressure nitrogen and air plasmas when seeded with potassium carbonate powder. Since the exact amount and uniformity of the seed material is seldom known to any degree of accuracy in flowing plasma systems, the aim was to develop methods which are relatively insensitive to these parameters. To avoid perturbations of the plasma the methods developed have been purely spectroscopic, employing only external optical probes.

The one year program involved both analytical and experimental methods. Externally measured lateral distributions of atomic spectral lines and molecular bands of the parent gases and atomic lines and the continuum of the seed material were converted to radial distributions of the emission coefficients by means of the usual inversion of the Abel integral equation. Number densities of each species of particles were computed for assumed concentrations of potassium seed on the assumption of local thermal equilibrium. The temperature dependence of the emission coefficients computed from these number densities were then used to convert the measured emission coefficients to radial temperature distributions.

The analytical methods developed in Section III were used to convert the spectral intensities measured by means of the apparatus described in Section II to emission coefficients. The experimental results in the form of radial temperature distributions obtained from measured emission coefficients are given and discussed in Section IV and conclusions and recommendations are given in Section V.

II. EXPERIMENTAL METHODS

A. APPARATUS

The experimental apparatus used throughout this investigation is shown schematically in Fig. 1. The auxiliary arc chamber shown was used only for secondary calibrations of the common spectral diagnostic system. Its primary function was in association with an independent experimental investigation. The physical arrangement of the apparatus is shown in the photograph of Fig. 2. The chemical bottles observable in the foreground of the photo are part of the scrubbing system required when operating with air to remove the NO after exhausting from the quench chamber. The spectrograph and central console which are physically located in the foreground, out of view in Fig. 2, are shown in the separate view of Fig. 3. Details of each major component of the experimental apparatus are given in the following sub-sections.

1. Plasma Jet

The initial configuration of the plasma jet designed specifically for this program is shown schematically in the full scale drawing of Fig. 4. This design was chosen because of the inherently stable plasma it can produce. The stability results from the proportionately small variation in arc length that can occur in this design. The jet was designed to operate in the range of 180 to 230 volts with current in the range of 50 to 175 amp. The volume flow rate with nitrogen and air ranged from 80 to 150 SCFH providing an appreciable range of average enthalpies. Initially the constrictor section consisted of six 1/4" thick water cooled copper plates upstream of the seed feeder plate and two similar constrictor plates between the feeder plate and the anode. The inside diameter of the entire constrictor was 1/4 in.

The average enthalpy of the first configuration, obtained from a

calorimetric energy balance, was much higher than that which corresponds with the 2500°K to 4000°K temperature range required to simulate the AEDC accelerator conditions. In order to reduce the enthalpy the inside diameter of the constrictor was increased to 0.344 inch so as to increase the wall losses. With this change the plasma became too unstable. In order to re-establish the stability the anode diameter was changed back to 1/4 inch. This second jet configuration is shown in Fig. 5.

Although the second configuration reduced the average enthalpy it was not sufficient to reach the desired temperature range. A modification to the third and final configuration shown in Fig. 6 was made by removing one of the upstream constrictor plates and extending the anode section so as to eliminate the two constrictor plates downstream of the seed feeder section. With these changes the axis temperature was reduced to about 5000°K. The addition of seed carrier gas and the seeder fluidizing gas reduced the operating temperature in the third configuration to the desired level.

2. Observation and Quench Chamber

The jet head was designed to exit into the observation section and quench chamber shown schematically in Fig. 7. In order to prevent the viewing windowfrom fogging, a stream of auxiliary gas was directed over the inside surface and into the the water cooled cylindrical chamber through a 1/8 in. by 3/8 in. viewing slot. The exit gas was first cooled by a nested-tube heat exchanger before being vented, or, in the case of air operation, passed through the chemical scrubbing system. No attempt was made to determine the quantity of heat transferred to the quench chamber or that which remained in the vented gases. Only the losses in the jet head were determined calorimetrically by means of electrode and constrictor section cooling water systems.

3. Seeding System

The seed material in the form of powdered K_2CO_3 was first fed

into the feeder constrictor plate through a Metco powder feed hopper using as carrier gas nitrogen in the case of the nitrogen plasma and oxygen in the case of the air plasma. With this simple feed system the radial distribution of continuous radiation emitted by the jet was found to have a strong oscillatory characteristic, as shown on the sample trace of Fig. 8, which was found to be synchronized with the dumping of the seed buckets of the powder feeder.

In order to improve the uniformity of the seeding process, the fluidizing system shown in Fig. 9 was installed. With this system, the powdered and dried K_2CO_3 was dropped from the upper center tube of the fluidizing chamber by means of the powder feeder. A swirling gas fed from the bottom caused the powder to be supported in a vortex near the exit of the feed tube with a much more uniform stream being carried up to the outlet at the top of the fluidizing chamber and into the feeder section of the plasma jet. Flowmeters were provided to properly meter the two flows into the fluidizer. The improvement brought about by the fluidizing system is demonstrated by the continuum trace of Fig. 8 which was measured after installation of the fluidizing system. In order to demonstrate the basic stability of the jet, a trace measured with the unseeded jet is also shown in Fig. 8.

4. Traversing Table and Calibration Arc

The transport table which supports the combined jet head and quench chamber also supports the low current calibration type carbon arc. This is a Bausch and Lomb, Euler type arc whose positive carbon crater is used as a calibration source. The table is constructed such that a single lens system is used for observing both the jet and the carbon crater. The displacement of the transport table in a direction normal to the spectral probe defined by the spectrograph and focussing lens as a combined optical system is translated by means of a precision linear potentiometer to the X axis of a Moseley X-Y recorder. With this apparatus, lateral distributions such as

those shown in Fig. 8 can be recorded while maintaining their proper relationship with respect to the jet axis.

5. Radiation Detection System

The radiation from the plasma was resolved in wavelength by means of an Ebert type spectrograph designed and constructed at Plasma Sciences Laboratories. The spectrograph has a first order dispersion of 8.3 Å/mm and is equipped for direct photomultiplier read-out on an X-Y recorder. The associated instrumentation was such that either lateral positions or wavelengths could be displayed on the X axis with integrated spectral intensities on the Y axis. Two EMI photomultiplier tubes were used, i.e., the 9558 B for work in the far red region of the spectrum and the 9502 B for work in the visible and U V regions. The latter was chosen to permit detection of the continuum down to extremely low radiation levels. Coupling from the PM tubes to the recorder was through an operational amplifier which also served as an impedance matching device. The lower limit of the detector sensitivity was about 10^{-19} watt/(cm^3-sr-sec^{-1}) for the continuum and 10^{-7} watt/(cm^3-sr) for potassium lines which represents a lower temperature limit of about 2500°K in the seeded plasma.

B. INTENSITY MEASUREMENTS

The principal experimental measurements were the lateral distributions of integrated intensities emitted by the pure and seeded nitrogen and air plasmas. Intensities of the atomic nitrogen lines, the first 4.5 Å increment, $\delta\lambda$, of the λ 3914 $N_2^+(1-)(0,0)$ band system, the λ 3922 and λ 5600 electron continuum and λ 4965, λ 5832 and λ 6939 KI lines were measured and inverted to true radial distributions of the emission coefficients as emitted by both nitrogen and air plasmas with and without seed over a range of average plasma jet enthalpies. These species of radiation are identified on the sample spectrum of Fig. 10.

In each measurement the background radiation was subtracted,

except of course in the case of the continuum, before the inversion process. Each measurement was calibrated on an absolute intensity scale by means of the carbon arc standard. To eliminate any possible errors due to window fogging by the seed material, the transmission of the window was measured at the beginning and end of each run. Only when the transmission remained constant were the data considered acceptable. The measured transmission was, of course, included in the final calibrations.

The symmetry of the measured traces was determined by folding about the best axis of symmetry which in almost all cases was very well defined. In cases where some asymmetry was observed the two wings of the distribution were averaged. The straight-forward Nestor-Olsen[1] method was used with a desk calculator to perform the necessary numerical integration of the inverted Abel integral equation. In all cases the plasma was assumed to be optically thin.

C. PLASMA JET OPERATING CHARACTERISTICS

The operating characteristics of the plasma jet that could be measured directly on external meters were the voltage, current, gas pressure and flow rates, and inlet and outlet water temperatures and flow rates. The jet was always operated into an atmospheric pressure plenum chamber where spectral observations were made at different defined positions measured from the nozzle exit. The positive pressure in the plasma never exceeded, at the very most, 10 psi and this only with the most restricted flow through the scrubbing system. Usually the positive pressure was less than 8 psi.

The operating characteristics of the jet are recorded for all runs in Table I where they are identified by the data book number, page number, and recorder trace number. These identifying numbers are included for identification on the experimental results presented in the following section. The volume gas flow rates have all been converted to mass flow rates of the various feed systems.

The seed flow by weight was determined by measuring the weight of material fed during the time of a run. The numbers recorded are the average values obtained by assuming a uniform feed rate. The average enthalpies were determined from measured cooling water flow rates, inlet and outlet temperatures and total gas mass flow rates. The rate of energy input to the gas stream was obtained by subtracting the calorimetrically measured jet losses from the total electrical power input. By assuming the total volume of gas to be uniformly heated, the tabulated static enthalpy was determined from the calorimetrically measured power into the gas and the measured mass flow rate. The average temperature is that obtained from computed compositions for pure air and nitrogen which corresponds with the measured average enthalpy. The "measured" temperature is the average of the axis values measured by spectroscopic means. Finally, the "position" represents the distance from the nozzle exit where the spectral probing was made. The jet configuration refers to the three configurations shown in Figs. 5, 6, and 7 respectively.

Since the emphasis in this investigation was on developing spectral diagnostic methods, it was considered more important and significant to compare temperatures measured simultaneously by several methods in the same volume element than to compare with the average temperature obtained by calorimetric means. For this reason, the gross jet thermal and electrical properties were not measured with nearly the same precision as the spatially and spectrally resolved optical radiative properties. This seems quite justified when one considers the difficulties encountered with any gas dynamic treatment of the properties of a subsonic jet.

III. ANALYTICAL METHODS

The analytical methods consisted of computing the plasma compositions in the range of 2000 to 6000°K for seeded nitrogen and air plasmas. The number densities were then used to compute the temperature dependence of the respective emission coefficients using existing transition probabilities. Each of these computations is described in detail in the following sub-sections.

A. SEEDED NITROGEN PLASMA COMPOSITION

The general equations developed for computing the composition of the seeded nitrogen plasma have taken into consideration the following species with the seed material considered as pure potassium.

$$K \rightleftharpoons K^+ + e^- \tag{1}$$

$$N_2 \rightleftharpoons 2N \tag{2}$$

$$N_2 \rightleftharpoons N_2^+ + e^- \tag{3}$$

$$N \rightleftharpoons N^+ + e^-. \tag{4}$$

For convenience in writing the respective equations the following partial pressures are defined:

$$P_1 \equiv P_K \qquad P_4 \equiv P_{K^+}$$

$$P_2 \equiv P_{N_2} \qquad P_5 \equiv P_{N_2^+}$$

$$P_3 \equiv P_N \qquad P_6 \equiv P_{N^+}$$

$P_e \equiv$ Partial pressure of electrons.

Under the assumption of local thermodynamic equilibrium at constant pressure the following relations hold:

$$P_2 = P_3^2/S_2 \tag{5}$$

$$P_4 = P_1 S_1/P_e \tag{6}$$

$$P_5 = P_2 S_3/P_e = P_3^2 S_3/(P_e S_2) \tag{7}$$

$$P_6 = P_3 S_4/P_e \tag{8}$$

where

$$S_1 = 6.58014 \times 10^{-7} T^{5/2} (Z_4/Z_1) \exp(-50373.3/T)$$

$$S_2 = 4.74455 \times 10^{-1} T^{5/2} (Z_3^2/Z_2) \exp(-113245.7/T)$$

$$S_3 = 6.58014 \times 10^{-7} T^{5/2} (Z_5/Z_2) \exp(-180802.7/T)$$

$$S_4 = 6.58014 \times 10^{-7} T^{5/2} (Z_6/Z_3) \exp(-168840.2/T)$$

and the Z's are the respective partition functions. Partition functions for nitrogen were taken from the Drellishak[2] Tables. The partition functions for the potassium atom were evaluated by summing

$$Z_1 = \sum_i g_i \exp(-E_i/T)$$

over the first six excited states using the energies and statistical weights given in NBS circular 467. The ground state statistical weight of the potassium ion was used, i.e., $Z_4 = g_0 = 1$. All of the partition functions used in this work are given in Table II.

With the equilibrium concentration by volume of potassium seed defined as

$$a \equiv (P_1 + P_4)/P \tag{9}$$

where P is the total pressure of the system, equations (5) through (8) in conjunction with the following conservation equations

$$P = P_e + \sum_{i=1}^{6} P_i \tag{10}$$

$$P_e = \sum_{i=4}^{6} P_i \quad , \tag{11}$$

define a system of seven equations and seven unknowns. For the general solution of this set it has been found convenient to use Eqs. (6), (9) and (11) to express P_1 and P_4 as functions of P_e as follows:

$$P_1 = P_e a P/(P_e + S_1) \tag{12}$$

$$P_4 = a P S_1/(P_e + S_1) \, . \tag{13}$$

By means of Eqs. (11), (12) and (13), Eq. (10) can be transformed to

$$P_e aP/(P_e+S_1) + P_3^2/S_2 + 2P_e - P = 0 \tag{14}$$

and Eq. (11) can be transformed to

$$aPS_1/(P_e+S_1) + P_3^2 S_3/P_e S_2 + P_3 S_4/P_e - P_e = 0. \tag{15}$$

By eliminating P_3 between Eqs. (14) and (15) a sixth degree polynomial in P_e is obtained in the following form which is amenable to computer solution:

$$P_e^6 + AP_e^5 + BP_e^4 + CP_e^3 + DP_e^2 + EP_e + F = 0 \tag{16}$$

with the constants given in terms of the seed ratio, equilibrium constants and total pressure as follows:

$$A = 2(S_1+2S_3)$$

$$B = -(2aMP+NS_2) + 2S_3(2S_3-P) + S_1(8S_3+S_1)$$

$$C = -2S_1(aMP+NS_2) - 2S_3(2aMP+NS_2) + 4S_3(S_1^2-S_3P) + 4S_1S_3(2S_3-P) + 2N^2S_2$$

$$D = a^2M^2P^2 - 4S_1S_3(aMP+NS_2) + S_3P(2aMP+NS_2) - NS_1^2S_2 + S_3^2P(P-8S_1)$$
$$+ 2S_1^2S_3(2S_3-P) + aPN(M+N)S_2 + N^2S_2(4S_1-P)$$

$$E = 2S_1S_3P(aMP+NS_2) - 2NS_1^2S_2S_3 + 2S_1S_3^2P(P-2S_1) + aPN(M+N)S_1S_2$$
$$-2N^2S_1S_2P + 2N^2S_1^2S_2$$

$$F = NPS_1^2S_2S_3 + S_1^2S_3^2P^2 - N^2S_1^2S_2P$$

with $M = S_1 - S_3$

$N = S_3 - S_4$.

For temperatures below 6000°K the relative magnitudes of the S_i are such that S_3 and S_4 can be set to zero. Under this assumption $M \rightarrow S_1$ and $N \rightarrow 0$ and Eq. (16) becomes

$$P_e^4 + 2SP_e^3 + (S_1^2-2aS_1P)P_e^2 - 2aS_1^2PP_e + a^2S_1^2P^2 = 0 . \tag{16a}$$

This assumption means that contributions to P_e from ionization of

the nitrogen molecules and atoms are negligible in comparison with the contribution from ionization of the potassium atom. A simpler approach which is consistent with the same assumptions but involving only a quadratic equation is obtained by separating completely the ionization process from the dissociation process. This is possible since the dissociation process contributes no electrons.

Since the partial pressures of electrons and potassium ions can be assumed equal at temperatures below 6000°K ($P_e = P_4$) Eq. (9) becomes

$$P_1 + P_e = aP. \tag{9a}$$

A combination of Eqs. (9a) and (12) gives the following desired second degree equation in P_e:

$$P_e^2 + P_e S_1 - aPS_1 = 0 \tag{17}$$

with a meaningful positive root for P_e. By combining Eqs. (9a) and (10) the following is obtained:

$$P_3^2 + P_3 P_2 + S_2 P_e + P(a-1) = 0 . \tag{18}$$

The positive root of this equation with P_e obtained from Eq. (17) gives the meaningful value for P_3. These values for P_e and P_3 can then be used with equations (12), (5), (7) and (8) to obtain the respective values of P_1, P_2, P_5 and P_6 even though the latter two have been neglected in computing P_e as has also P_3.

Values of the respective partial pressures have been obtained on a desk calculator for a 1 atm plasma in the temperature range 2000°K to 6000°K and seed concentrations by volume (a) ranging from 0.01 to 0.001. The corresponding number densities and seed concentrations by weight (b) are tabulated in Table III. The numbers for a=0 were taken directly from Drellishak's[2] Tables for comparison. The relationship between the two concentrations is

$$b = 1/\left[1 + \left(\frac{1-a}{a}\right) M_{N_2}/M_K\right]$$

where M_K and M_{N_2} are the molecular weights of potassium and nitrogen.

B. SEEDED AIR PLASMA COMPOSITION

The general equations developed for computing the composition of the seeded air plasma have taken into consideration the following species with the seed material considered to be pure potassium:

$$K \rightleftharpoons K^+ + e^- \qquad O_2 \rightleftharpoons 2O$$

$$N_2 \rightleftharpoons 2N \qquad O_2 \rightleftharpoons O_2^+ + e^-$$

$$N_2 \rightleftharpoons N_2^+ + e^- \qquad O \rightleftharpoons O^+ + e^-$$

$$N \rightleftharpoons N^+ + e^- \qquad NO \rightleftharpoons N + O$$

$$NO \rightleftharpoons NO^+ + e^- \ .$$

For convenience in writing the respective equations and equilibrium constants, the following partial pressures are defined:

$$P_1 \equiv P_K \qquad P_7 \equiv P_{O_2}$$

$$P_2 \equiv P_{N_2} \qquad P_8 \equiv P_O$$

$$P_3 \equiv P_N \qquad P_9 \equiv P_{O_2^+}$$

$$P_4 \equiv P_{K^+} \qquad P_{10} \equiv P_{O^+}$$

$$P_5 \equiv P_{N_2^+} \qquad P_{11} \equiv P_{NO}$$

$$P_6 \equiv P_{N^+} \qquad P_{12} \equiv P_{NO^+} \ .$$

Under the assumption of local thermodynamic equilibrium at constant pressure the following relations hold:

$$S_1 = P_e P_4/P_1 \qquad S_4 = P_e P_6/P_3 \qquad S_7 = P_e P_{10}/P_8$$

$$S_2 = P_3^2/P_2 \qquad S_5 = P_8^2/P_7 \qquad S_8 = P_3 P_8/P_{11}$$

$$S_3 = P_e P_5/P_2 \qquad S_6 = P_e P_9/P_7 \qquad S_9 = P_e P_{12}/P_{11} \tag{19}$$

$$P = P_e + \sum_{i=1}^{12} P_i \qquad P_e = \sum_{i=4}^{12} P_i \qquad a \equiv (P_1+P_4)/P \ .$$

The above set of twelve equations can be reduced to the following three to constitute the complete solution:

$$P_3^2S_3S_5S_8(P_e+S_1) + P_3S_2S_4S_5S_8(P_e+S_1) + P_8^2S_2S_6S_8(P_e+S_1)$$
$$+ P_8S_2S_5S_7S_8(P_e+S_1) + P_3P_8S_2S_5S_9(P_e+S_1) + aPS_1S_2S_5S_8P_e \tag{20}$$
$$- P_e^2S_2S_5S_8(P_e+S_1) = 0$$

$$P_3^2S_5S_8(P_e+S_3) + P_3S_2S_5S_8(P_e+S_4) + P_3P_8S_2S_5(P_e+S_9)(1-\xi)$$
$$- \xi P_8^2S_2S_8(P_e+S_6) - \xi P_8S_2S_5S_8(P_e+S_7) = 0 \tag{21}$$

$$P_3^2S_5S_8(P_e+S_1) + P_3S_2S_5S_8(P_e+S_1) + P_3P_8S_2S_5(P_e+S_1)$$
$$+ P_8^2S_2S_8(P_e+S_1) + P_8S_2S_5(P_e+S_1) + aPP_eS_2S_5 - PS_2S_5(P_e+S_1) \tag{22}$$
$$+ 2P_eS_2S_5(P_e+S_1) = 0$$

where P_e, P_3, P_8 are the respective partial pressures of electrons, nitrogen atoms and oxygen atoms. The S_i are the defined equilibrium constants, a is the seed concentration by volume at equilibrium temperature and

$$\xi = \frac{P_2+P_3+P_5+P_6+P_{11}+P_{12}}{P_7+P_8+P_9+P_{10}+P_{11}+P_{12}}$$

is the equilibrium ratio of the sum of all partial pressures of species containing nitrogen to the sum of all partial pressures of species containing oxygen.

In the calculation of P_e the contribution of electrons from ionization of molecules and atoms of both nitrogen and oxygen can be neglected in the range 2000°K to 6000°K when seed is present. The contribution of electrons from the ionization of NO, though small, can not be neglected. With these assumptions the three general equations involving P_3, P_8 and P_e can be simplified to

$$P_3P_8 = S_8\left[P_e^2(P_e+S_1) - aS_1PP_e\right]/\left[S_9(P_e+S_1)\right] \tag{20a}$$

$$P_3^2S_5S_8P_e + P_3S_2S_5S_8P_e + P_3P_8S_2S_5(P_e+S_9)(1-\xi) - \xi P_8^2S_2S_8P_e - \xi P_8S_2S_5S_8P_e = 0 \tag{21a}$$

Same as Equation (22). (22a)

It is possible to eliminate either P_3 or P_8 between Eqs. (20a), (21a) and (22a). In so doing, P_3 and P_8 can be obtained as a function of P_e only, as follows:

$$P_8^2S_8P_e(P_e+S_1)(1+\xi) + P_8S_5S_8P_e(P_e+S_1)(1+\xi) + mS_5(P_e+S_1)\left[P_e\xi - S_9(1-\xi)\right] + S_5S_8P_e\left[(2P_e-P)(P_e+S_1) - aPP_e\right] = 0 \tag{23}$$

$$P_3^2S_8P_e(P_e+S_1)(1+\xi) + P_3S_2S_8P_e(P_e+S_1)(1+\xi) + mS_2(P_e+S_1)\left[P_e+S_9(1-\xi)\right] + \xi S_2S_8P_e\left[(2P_e-P)(P_e+S_1)-aPP_e\right] = 0 \tag{24}$$

where $m=P_3P_8$ is seen by Eq. (20a) to be a function only of P_e, S_i and a. Equations (20a), (23) and (24) can, in principle, be combined to give an equation in P_e; however this can only be accomplished numerically by means of an electronic computer. From such a solution for P_e, all of the other partial pressures can be computed. A very good first approximation can be obtained by assuming that, except for the dilution effect, P_3 and P_8 are not affected by the presence of seed. From the seeded nitrogen data of Table III it can be seen that this assumption is certainly valid and practical since it leads to the following simple form of Eq. (20a):

$$P_e^3 + P_e^2S_1 - P_e(aS_1P+P_3P_8S_9/S_8) - P_3P_8S_9S_1/S_8 = 0. \tag{20b}$$

This equation with the following expressions for the equilibrium constants was used, along with S_1, S_2, S_3 and S_4 given above to compute the composition of the seeded 1 atm air plasma.

$$S_5 = 5.79673 \times 10^{-1}T^{5/2}(Z_8^2/Z_7)\exp(-59368/T)$$

$$S_6 = 6.58014 \times 10^{-7}T^{5/2}(Z_9/Z_7)\exp(-141795/T)$$

$$S_7 = 6.58014 \times 10^{-7} T^{5/2} (Z_{10}/Z_8) \exp(-158037/T)$$

$$S_8 = 5.22682 \times 10^{-1} T^{5/2} (Z_3 Z_8/Z_{11}) \exp(-75506/T)$$

$$S_9 = 6.58014 \times 10^{-7} T^{5/2} (Z_{12}/Z_{11}) \exp(-107445/T).$$

The additional partition functions needed for these computations are given in Table II. The computed results are given as number densities in Table IV along with the concentration by volume (a) and by weight (b) of the seed material. The relation between the two concentrations is as given above with the molecular weight of air replacing that of nitrogen.

C. EMISSION COEFFICIENTS

In order to compute the emission coefficient for a constant concentration by weight of the seed material it was first necessary to cross-plot the number densities which were computed at constant concentration by volume. The reason for this approach was to avoid the more complex form of the composition equations when expressed in terms of the weight ratio. Emission coefficients for each of the species of radiation investigated are treated in the following sub-sections, starting with those species which occur at the highest temperatures.

1. Atomic Nitrogen Lines

Two of the strongest atomic lines observed in the nitrogen plasma are $\lambda 4935$ and $\lambda 7469$. These lines are chosen because they are quite free of interference from other lines or band systems as shown in the sample spectrum traces of Fig. 10. They also have quite different upper energy levels which make them useful for checking equilibrium conditions. The emission coefficients have been computed only for the pure nitrogen and air plasmas since they fall below the lower limits of the detector in the temperature range encountered with the seeded plasma, i.e. 10^{-9} watt/(cm^3-sr).

Emission coefficients for the two lines have been computed from

$$\epsilon = 1.582 \times 10^{-16} (AgN/Z_3 \lambda) \exp(-E_m/T) \tag{25}$$

where for λ in Å, N in cm^{-3} and A in sec^{-1} the units are watts/ (cm^3-sr). The constants used for the two lines are

λ	4935	7469
g	2	4
$A(sec^{-1})$	1.58×10^6	1.61×10^7
$E_m(°K)$	153206	139210

In earlier calculations[3] the transition probabilities were erroneously taken for the total multiplets. The corrected probabilities tabulated here are now accepted by the NBS as correct. Using the number densities for pure nitrogen and air plasmas published by Drellishak[2], et.al., and Hilsenrath[4], et.al., the emission coefficients in Figs.11 and 12were computed. The partition functions were taken from Table II of this report.

2. Molecular ion Band, λ 3914 $N_2^+(1-)(0,0)$

A portion of this band system recorded near the head as emitted by the high temperature pure nitrogen jet on the axis is shown in Fig. 13 . The head portion of the band indicated by $\delta\lambda$ on Fig. 13 is composed of the first 26 components of the P branch which do not overlap the R branch. The total emission coefficient for this wavelength increment of the band has been computed by means of the following equation:

$$\epsilon = C \frac{N_2}{Z_2} \exp(-E_e/T) \sum_{K'=0}^{25} \left\{ \frac{2(K'+1)}{\lambda_{K'}^4} \left[1 - \frac{1}{(2K'+1)(2K'+3)} \right] \beta_{K'} \exp\left[-B_0 K'(K'+1)/T \right] \right\} \qquad (26)$$

where K' is the rotational quantum number of the upper state and

$$C = 16\pi^3 cg \times 10^{-7} \bar{R}_e^2 q_{v'v''}/3$$

$$= 2.9745 \times 10^6 \bar{R}_e^2 q_{v'v''}$$

$$g = 6$$

$$E_e = 36635.7°K$$

$$B_0 = 2.98308°K$$

$$\beta_{K'} \begin{cases} = \frac{1}{2} \text{ for } K' \text{ even} \\ = 1 \text{ for } K' \text{ odd.} \end{cases}$$

The value of $\bar{R}_e^2 q_{v'v''}$ used in this calculation was taken as 2.36×10^{-36} which was obtained from the average of the seven published values for the transition probabilities given in Ref. 5. With λ in cm and number density in cm^{-3} the units of $\bar{R}_e^2 q_{v'v''}$ are such that the emission coefficient is in watt/(cm^3-sr).

The computed coefficients for pure nitrogen and air plasmas over the temperature range of 2000°K to 10,000°K are given in Figs.11and 12. For these calculations the number densities for nitrogen were taken from Ref. 2 and those for air from Ref. 4. Similar results for seeded nitrogen and air plasmas are plotted in Figs.14 and 15. For these calculations the cross-plotted number densities from Tables III and IV were used for constant values of the mass ratio of seed to gas. For direct comparisons the curves for no seed are repeated from the previous figures.

3. Electron Continuum

The Kramers-Unsöld equation in the form

$$\epsilon = 5.41 \times 10^{-46} Z_{eff}^2 N_e^2 / T^{\frac{1}{2}} \tag{27}$$

has been used to compute the emission coefficient for the electron continuum emitted by the seeded plasmas. With electron number densities N_e in cm^{-3} and T in °K the units are in watt/(cm^3-sr-sec^{-1}). The effective charge of the retarding ions, Z_{eff}, is taken as 1 since only singly charged ions can exist at the low temperatures encountered here. Since the electron number densities are practically the same for both nitrogen and air seeded plasmas as can be seen in Tables III and IV, the single set of curves in Fig.16 serves for both plasmas.

According to Eq. 27 the computed continuum is independent of frequency. In order to apply the computed results to experimental data it is necessary to multiply by a factor $\frac{c\Delta\lambda}{\lambda^2}$ where $\Delta\lambda$ is the increment of wavelength covered by the detector at the measured wavelength λ. In all experimental measurements carried out here

$\lambda = 3922$ Å thus the scales of the computed coefficients must be multiplied by a factor of $\sim 10^{12}$ in order to convert them to watt/(cm^3-sr) for a more direct comparison with band or line intensity measurements using approximately the same slit width.

The unique maximum reached by the continuum at about 5000°K is the well known normal value which represents the temperature at which the increase in emission due to increased ionization is just balanced by the decrease caused by increasing temperature. The location of the peak on the temperature scale as well as its absolute maximum are both sensitive to the amount of seed present. In principle, because of the extreme sensitivity of the absolute value of the emission coefficient and relative insensitivity of the location on the temperature scale, the measurement of such a peak could serve to determine the concentration of seed material in a plasma. In practice this is not true since the temperature range of seeded operations is generally below the normal value and the accuracy of the measured radial distribution even in cases where the normal temperature is exceeded is not sufficient to properly interpret an off axis peak.

4. Atomic Potassium Lines

The observed groupings of atomic potassium lines into "quartets" is at first confusing when one realizes that there are only doublet and triplet multiplet structures in the atom. The arrangement of lines in groups of four as, for example, λ 5783, λ 5802, λ 5813 and λ 5832 is the result of the grouping of the $3^2S \rightarrow 2^2P$ doublet and the $5^2D \rightarrow 2^2P$ triplet under conditions where the observed λ 5832 line is in actuality an unresolved pair of lines, one from each multiplet, with only ~ 0.2 Å wavelength difference. The orientation within the pseudo quartets is always such that the unresolved line-pair of the triplet is well resolved from, and falls at the long wavelength side of, the group.

Because of the relatively small energy differences for the observed multiplets of potassium, only absolute emission coefficients for the discrete atomic lines or line pairs can give satisfactory accuracy in temperatures determined from measured emission coefficients in the temperature range of 2500 to 4000°K. For this reason the absolute emission coefficients for selected lines and line pairs have been determined from the computed seeded plasma compositions and partition functions.

Since absolute transition probabilities are available only for the total multiplets[6] it was first necessary to develop a method for writing the absolute emission coefficient for each line of the multiplet in terms of the known line parameters and the total transition probability. Throughout this development reference will be made to the general structure of the multiplet energy levels as shown below where the three lines are designated by the subscripts 1, 2 and 3.

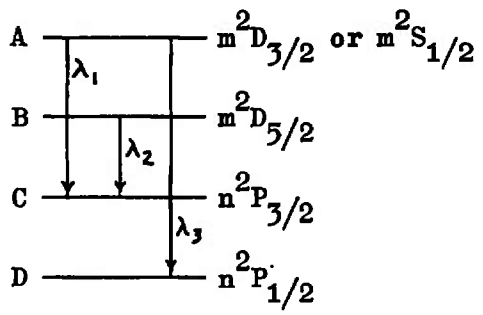

The total emission coefficient for the multiplet can be written in terms of the individual lines as

$$\epsilon_T = 1.582 \times 10^{-16}(N_1/Z_1) \sum_{i=1}^{3} (A_i g_i/\lambda_i)\exp(-E_m^i/T) . \tag{28}$$

In order to write this in terms of a total transition probability it is necessary to define an average energy $\bar{E}_m$ and wavelength $\bar{\lambda}$ such that

$$\epsilon_T = 1.582 \times 10^{-16}(N_1/Z_1)(A_T g_T/\bar{\lambda})\exp(\bar{E}_m/T) . \tag{29}$$

Such an average energy for both the upper and lower levels can be written as

$$\bar{E}_m \equiv \frac{g_A E_A + g_B E_B}{g_A + g_B} \quad ; \quad \bar{E}_n \equiv \frac{g_C E_C + g_D E_D}{g_C + g_D} \quad .$$

With these definitions the average wavelength can be written in terms of the average energies in °K as

$$\frac{1}{\bar{\lambda}} \equiv \frac{(\bar{E}_m - \bar{E}_n)}{1.4388} \quad .$$

A comparison of Eqs. (28) and (29) shows that

$$(A_T g_T/\bar{\lambda}) = (A_1 g_1/\lambda_1) + (A_2 g_2/\lambda_2) + (A_3 g_3/\lambda_3) \tag{30}$$

when the defined average quantities can be made. The transition probability ratios can be written in terms of relative line strengths as

$$(A_2/A_1) = (S_2/S_1)(g_1/g_2)(\lambda_1/\lambda_2)^3 \quad ; \quad (A_3/A_1) = (S_3/S_1)(g_1/g_3)(\lambda_1/\lambda_3)^3. \tag{31}$$

A simultaneous solution of Eqs. (30) and (31) leads to the following expressions for the individual transition probabilities in terms of the statistical weights, relative line strengths, wavelengths and the total probability:

$$A_1 = \frac{A_T g_T}{g_1 \bar{\lambda}} f(\lambda_i) \quad ; \quad A_2 = \frac{A_T g_T}{g_2 \bar{\lambda}} \frac{S_2}{S_1} f(\lambda_i) \quad ; \quad A_3 = \frac{A_T g_T}{g_2 \bar{\lambda}} \frac{S_3}{S_1} f(\lambda_i) \tag{32}$$

where

$$f(\lambda_i) = \left[\frac{1}{\lambda_1} + \frac{1}{\lambda_2}\left(\frac{\lambda_1}{\lambda_2}\right)^3 \frac{S_2}{S_1} + \frac{1}{\lambda_3}\left(\frac{\lambda_1}{\lambda_3}\right)^3 \frac{S_3}{S_1}\right]^{-1} \quad .$$

Since in the case of the $m^2D \rightarrow n^2P$ triplet $\lambda_1 \approx \lambda_2$ and in the case of the $m^2S \rightarrow n^2P$ doublet λ_2 does not exist it is practical to simplify $f(\lambda_i)$ to

$$f(\lambda_1 \lambda_3) = \lambda_1 \lambda_3 \left[1 + \frac{S_2}{S_1}\lambda_3 + \frac{S_3}{S_1}\lambda_1\left(\frac{\lambda_1}{\lambda_3}\right)^3\right]^{-1} \quad . \tag{33}$$

The total emission coefficient for the unresolved line pair of the triplet which falls at the wavelength $\lambda_1 = \lambda_2$ can now be written in terms of the total multiplet transition probability A_T, the total statistical weight g_T, the average wavelength $\bar{\lambda}$, average energy $\bar{E}_m$ and the simplified wavelength function $f(\lambda_1\lambda_3)$ as

$$\bar{\epsilon}_1 = \epsilon_1 + \epsilon_2 = 1.582 \times 10^{-16} \frac{N_1}{Z_1} g_T \left(1+\frac{S_2}{S_1}\right) A_T \frac{f(\lambda_1 \lambda_3)}{\lambda_1 \bar{\lambda}} \tag{34}$$

where the wavelengths are in Å and ϵ is in watt/(cm^3-sr).

Everything developed above for the $m^2D \rightarrow n^2P$ triplets can be applied directly to the $n^2S \rightarrow n^2P$ doublets by simply setting E_B, A_2 and S_2 equal to zero. All of the parameters required for computing the absolute emission coefficients for all of the lines or line pairs used in this investigation are given in Tables V, VI and VII. The computed emission coefficients for the listed lines are plotted as a function of temperature for a range of seed concentrations in Figs.17 through 20.

D. TEMPERATURE DETERMINATION

Because of the greater sensitivity (see ref. 5) of the absolute intensity of a line or band system to temperature than the ratio of lines or band components, only absolute emission coefficients have been used to determine plasma temperatures in this investigation. All measured integrated intensity distributions were first inverted to radial distributions of the emission coefficient using a conventional method[1] for the numerical solution of the inverted Abel integral equation.

A graphical comparison of the computed temperature and the measured radial distributions of a given species of radiation yields the radial distribution of the temperature by elimination of the emission coefficient as a common parameter. By repeating this process with the several species of radiation emitted from the same volume element of a plasma a check on the accuracy of

the measurement is possible. Because of the extreme sensitivity of the absolute emission coefficient to temperature at the lower levels of temperature encountered in seeded plasmas the method yields very satisfactory results. This feature also makes the method relatively insensitive to errors in the actual concentration and uniformity of the seed material present even though this concentration is required in the theoretical calculations.

IV. DISCUSSION OF RESULTS

The direct experimental results are lateral distributions of the emitted integrated spectral intensities such as, for example, the traces shown in Fig. 8. Such traces were first symmetrized, smoothed and then inverted to radial distributions of the emission coefficients by the Nester-Olsen[1] inversion method. By comparing the inverted distributions with the computed temperature distributions of the emission coefficients discussed in Section III the final results in the form of radial temperature profiles were obtained.

The analytical methods described in Section III were first applied to the high temperature pure nitrogen jet. The graphical method for determining the radial temperature from the measured emission coefficient of the $\delta\lambda$ increment of the $N_2^+(1-)(0,0)$ band system is illustrated in Fig. 21. Here the computed temperature dependence of the emission coefficient has been normalized to have the same maximum value as that measured. For a given value of ϵ, the common coordinates, (T,r), are obtained from the two curves $\epsilon(T)$ and $\epsilon(r)$ by the Larenz[7] method. In the region where double values exist the highest temperature is associated with the smallest radius based on the very reasonable assumption that $T(r)$ is a monotonically decreasing function. Since the location of the peak in the $\epsilon(T)$ distribution is determined essentially by the electron temperature through the electronic state exponential function, the temperature distribution obtained by this relative method should be more nearly equal to the electronic temperature than to the rotational temperature.

The numerical factor, $\bar{R}_e^2 q_{v'v''}$, needed to normalize the two curves of Fig. 21 was found to be 2.27×10^{-37} which is just about an order of magnitude lower than the value obtained

from the electronic oscillator strengths. To further investigate this apparent non-equilibrium, relative intensities of rotational components of the band system well separated in quantum number have been investigated. The temperature determined in this manner should be independent of the composition computations and more nearly equal to the heavy particle temperature. The complete wavelength distribution of the λ 3914 band, a portion of which is shown in Fig. 13, measured in integrated radiation emitted on the axis of the high temperature jet has shown the R branch components with K'=2 and K'=70 to be in the approximate ratio of 1.9 to 1. From the computed equilibrium ratio shown in Fig. 22 this measured ratio would mean an axis rotational temperature of $\sim$9400°K. Since the wavelength response of the detector system falls off towards shorter wavelengths, the measured ratio, when properly corrected for this effect, would be even smaller leading to a still higher temperature.

To further check the equilibrium condition, temperature distributions were also determined by a similar comparison with the absolute emission coefficients for two atomic spectral lines measured in the same volume element of the plasma. The results are compared with those determined from the band system in Fig. 23. The observed excellent agreement in temperatures determined from the atomic lines, whose excitation energies differ by 1.2 eV, demonstrates the existence of excitational equilibrium at the electron temperature. The close agreement between these temperatures and that determined from the normalized emission coefficients of the band system demonstrates excitational equilibrium for the electronic state of the molecule. The equilibrium excitation of the rotational state of the molecule at nearly the same temperature, as discussed above, lends considerable support to the assumption of local thermodynamic equilibrium.

There remains, however, the observed discrepancy between the

measured $\bar{R}_e^2 q_{v'v''}$ factors of this experiment and that obtained from the literature. This discrepancy is translated into a temperature error by comparing the temperature determined from the absolute measured and computed emission coefficients of the band system with those discussed above. This comparison is made graphically in Fig. 23. The discrepancy appears to remain with the absolute value of $\bar{R}_e^2 q_{v'v''}$ which can be resolved only with more accurate experimental measurements in sources having different excitation mechanisms.

A comparison of the computed emission coefficients discussed in Section III demonstrates quite positively that for seeded plasmas in the 2500°K to 4000°K temperature range the species of radiation that must be used for temperature measurements are the continuum and the potassium seed lines themselves. The practical lower limit for detection of the continuum with the apparatus used here was $\sim 10^{-19}$ watt/(cm^3-sr-sec^{-1}). This corresponds with a band or line intensity of about 10^{-7} watt/(cm^3-sr). In order to separate a discrete radiation from the background continuum its emission coefficient would have to be at least of the order of 10^{-6} watt/(cm^3-sr) or higher. For the seeded air plasma, this would correspond with a temperature of about 5000°K for any seed rate. At that temperature, however, the continuum intensity will reach its maximum which is nearly four orders of magnitude higher, so that the lower temperature limit for using the band system in seeded plasmas is more realistically 6000°K. On the other hand, for a seed ratio b=0.014 the continuum intensity reaches the lower limit at $\sim$ 2500°K where the emission coefficient of the λ 6939 KI line is in the range of 10^{-3} watt/(cm^3-sr).

At the lowest temperatures measured in this investigation, it was always possible to detect the increment, $\delta\lambda$, of the band system above the level of the continuum in the seeded plasma. The measured emission coefficients for the band increment were of the order of

10^{-4}watt/(cm^3-sr) or higher which correspond with temperatures in the range of 5000°K to 7000°K whereas the continuum and seed line temperatures were in the range of 2500°K to 4000°K. It would appear that some mechanism exists in the seeded plasma for exciting this band system which is not a thermal process as was assumed when computing the absolute value of the emission coefficient. In addition, the above mentioned discrepancy in the normalizing factor is in the wrong direction to account for this difference. For these reasons it was not possible to procede with the original plan of successively calibrating first the band increment against the nitrogen atomic lines, then the potassium seed lines against the band system and finally, the continuum against the seed line as the equilibrium temperature was lowered.

In principle, the rotational temperature could be determined from a Boltzmann plot of the resolved rotational components of the band in the same manner as is done with the electron beam excitation in the Muntz method. However, since the aim in this investigation was toward a simplified detection system to be developed eventually for diagnosing the non-symmetrical accelerator plasma, this basic problem was not pursued further under this contract. Emphasis was placed, instead, on using the much less complex spectrum of the potassium seed lines and the free-electron continuum as the sources of radiation to be used in the finally selected diagnostic system.

Temperature distributions determined independently from the measured continuum at two different seed ratios in air are shown in Fig. 24 to demonstrate the excellent reproducibility of the method. A comparison of temperature distributions determined from the continuum at two different wavelengths and from three different atomic lines of the potassium seed, all at the same seed ratio in air, are shown in Fig. 25. Similar results for a different seed ratio in nitrogen including the results of an attempt to determine temperatures by the line ratio method are shown in Fig. 26. Finally, results for still a different seed ratio in air are shown for a

slightly lower temperature range in Fig. 27.

These results indicate that the jet temperature is not very sensitive to the precise amount of seed material present in the range of 0.5 to 1% by weight. There is a tendency for the temperatures determined from the measured continuum to be consistently higher than those determined from the measured atomic lines of the seed material. The observed flattening of the temperature distributions obtained from the potassium lines indicates that self-absorption may be effective in reducing the intensity of the lines emitted along the plasma diameter. Such absorption could well be the cause of the lower temperatures obtained from the potassium line emission.

The enlarged temperature scales used in Figs. 25-27 tend to exaggerate the errors. An arithmetic average of the axis values for the nine distributions given in Figs. 25 and 26 amounts to T_o=3050± 4%. It is quite certain that an accurate treatment of the self-absorption would improve this. Certainly additional measurements of the continuum along would lead to a more reproducible value at the higher level. This observed accuracy in measured temperatures is consistent with that predicted by the theoretical curves of Section III. For example, at a temperature of 3000°K, a variation of seed concentration between 0.005 and 0.010 at a specified level of the emission coefficient would lead to an error of ± 2% for the continuum and ± 4% for the λ 6939 KI line. At a constant value of seed concentration a factor of 2 error in the measured emission coefficient would lead to the same errors in determined temperatures.

V. CONCLUSIONS AND RECOMMENDATIONS

The most general conclusion that can be drawn from the results of this investigation is that the continuous radiation emitted by the seeded plasma in the temperature range of 2500°K to 4000°K can be employed with an accuracy of better than ± 5% to determine seeded plasma temperature distributions by means of non-perturbing spectral probes. The method developed is relatively insensitive to fluctuations in seed concentration and uniformity as well as to errors in measured intensity. Radiation emitted in atomic spectral lines of the seed material can also be used but with only approximately half of the accuracy obtained with the continuum. The accuracy of both methods increases with decreasing temperature. In the above mentioned temperature range the continuous background radiation completely masks any species of radiation characteristic of the parent gas. This is consistent with the conclusion that the free electron and potassium atom concentrations can be computed in this range without considering the ionization of any parent gas particles.

It is recommended that diagnostic instrumentation be developed for rapid scanning of experimental plasma sources, recording simultaneously the spectrally resolved radiation emitted by the seed lines and the continuum. Absorption corrections for the seed lines should be made in order to finally check the accuracy of the continuum measurement for determining temperatures. The scanning device and dispersing element should be designed to be compatible with the high power plasma seeded jets and $\vec{J} \times \vec{B}$ accelerator system under development at AEDC. The entire diagnostic system should be thoroughly tested and calibrated with a more stable plasma jet system of the type used in this investigation before attempting to apply it to the AEDC facility.

It is also recommended that concurrent with the development

of practical diagnostic tools the still existing discrepancy between the measured and computed emission coefficients for the λ 3914 $N_2^+(1-)(0,0)$ band system be further investigated. Such an investigation would involve measurements of the absolute emission coefficients of either resolved rotational quartet groups or of the band head increment in pure nitrogen plasmas under different conditions of excitation, such as the stabilized dc jet and the rf induction plasma. When the existing discrepancy between the measured and published $\bar{R}_e^2 q_{v'v''}$ factor has been resolved the enhancement of the band radiation in the presence of seed should be thoroughly investigated.

In the event that the electronic state excitation is found not to be in thermal equilibrium with the gas temperature, the heavy particle temperature should at least be determined from the rotational structure of the band system emitted by the seeded plasma as a final check of the lower temperatures obtained from the seed material itself. In addition to providing the final check on the recommended diagnostic system, such an extension of the program would seem justified because of the importance of this band system to the diagnostic methods being considered for the expansion section of the AEDC accelerator.

REFERENCES

1. Nestor, O. H. and Olsen, H. N., "Numerical Methods for Reducing Line and Surface Probe Data," Soc. Ind. Appl. Math. Rev. 2, 200 (1960).

2. Drellishak, K. S., Aeschliman, D. P., and Cambel, A. B., "Tables of Thermodynamic Properties of Argon, Nitrogen and Oxygen Plasmas," AEDC-TDR-64-12 (Jan 1964).

3. Bodoia, J. R., Caron, A. P., Duckworth, G. D., Maldonado, C. D., and Olsen, H. N., "A Study of Spectral Diagnostic Methods for a $\vec{J} \times \vec{B}$ Wind Tunnel Driver," AEDC-TR-65-236 (Dec 1965).

4. Hilsenrath, J. and Klein, M., "Tables of Thermodynamic Properties of Air in Chemical Equilibrium Including Second Virial Corrections from 1500° to 15,000°K," AEDC-TR-65-58 (Mar 1965).

5. Olsen, H. N., Eckert, H. U. and Kelly, F. L., "Spectral Diagnostics of a Flowing Air Plasma," AEDC-TR-67-146 (July 1967).

6. Anderson, E. M. and Zilitis, V. A., "Oscillator Strengths for Sodium and Potassium Atoms Calculated by a Semiempirical Method," Opt. and Spect. 16, 99 (1964).

7. Larenz, W., "Concerning a Method for the Measurement of Very High Temperatures in Nearly Transparent Plasmas," Z. Physik 129, 327 (1951)

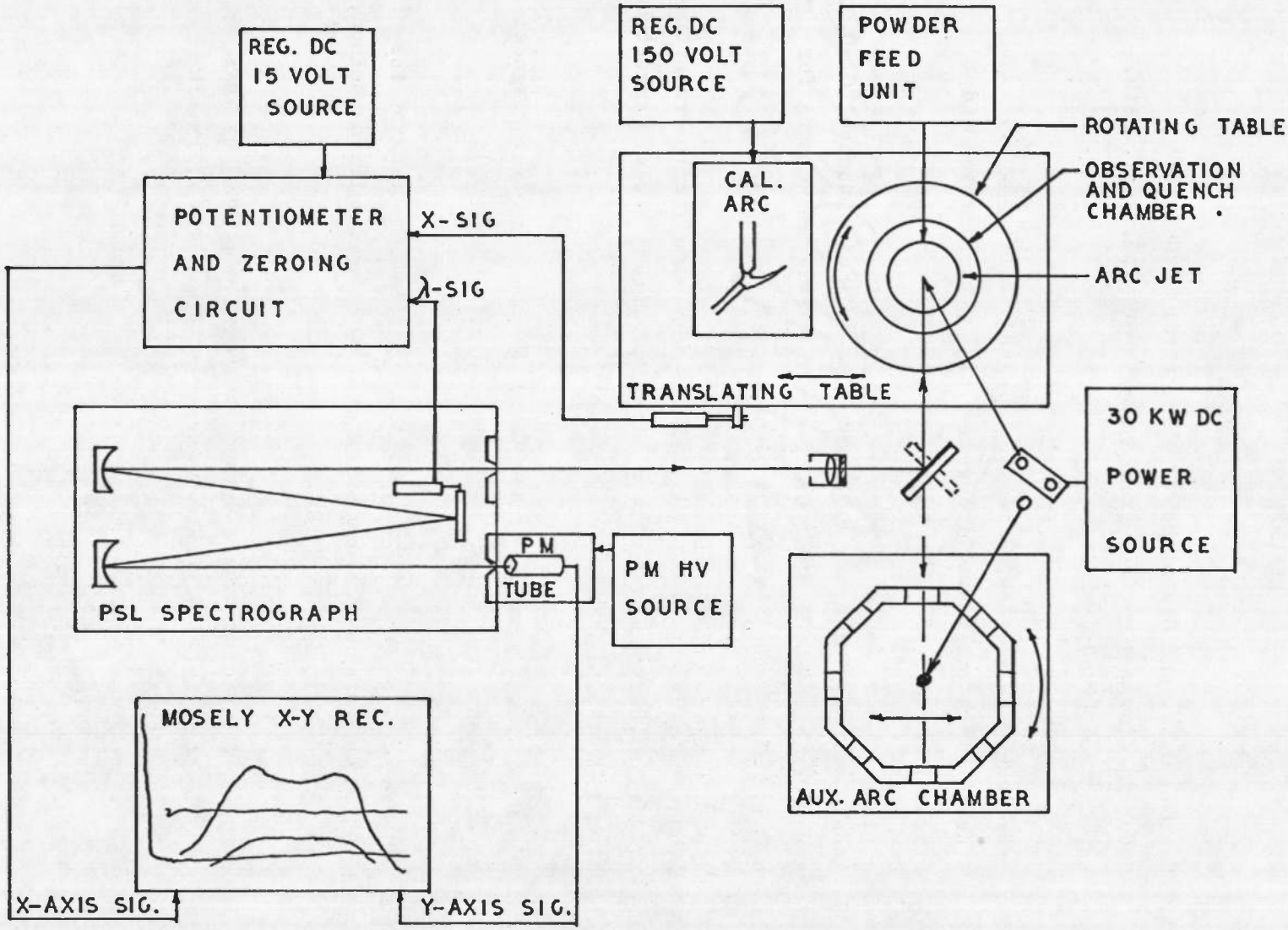

Fig. 1. Schematic diagram of experimental apparatus.

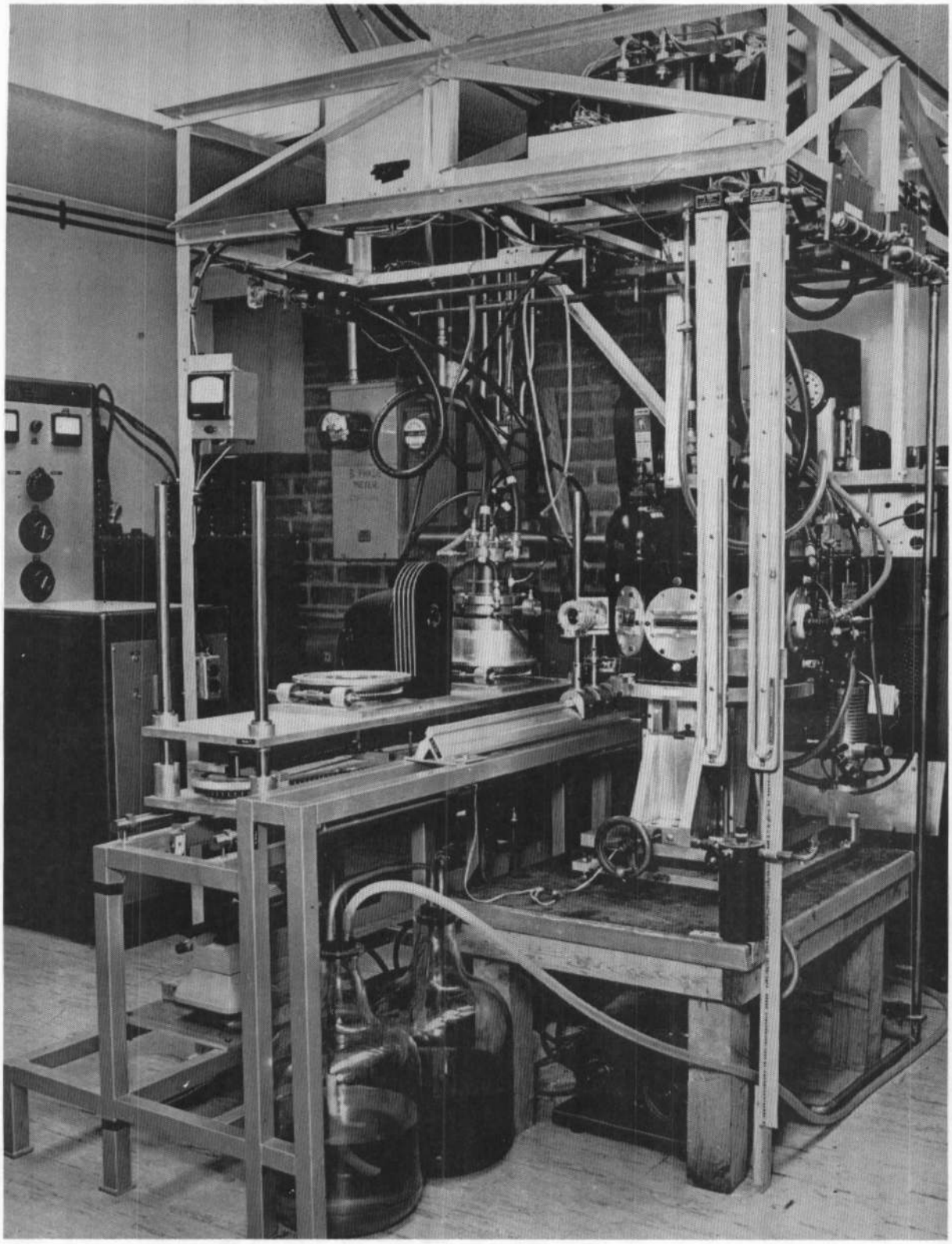

Fig. 2. Photograph of arc apparatus shown schematically in Fig. 1.

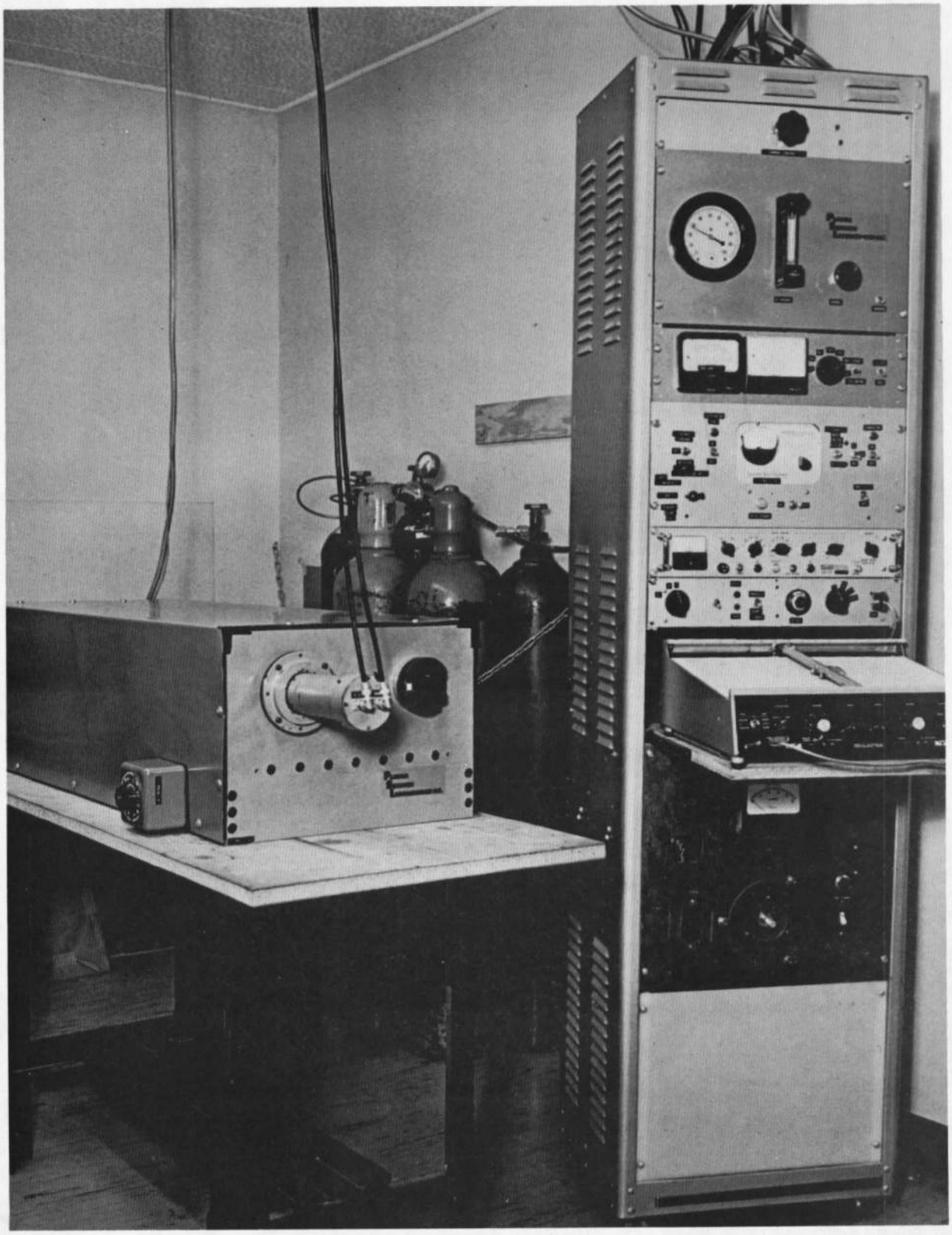

Fig. 3. Photograph of spectrograph and recording apparatus shown schematically in Fig. 1.

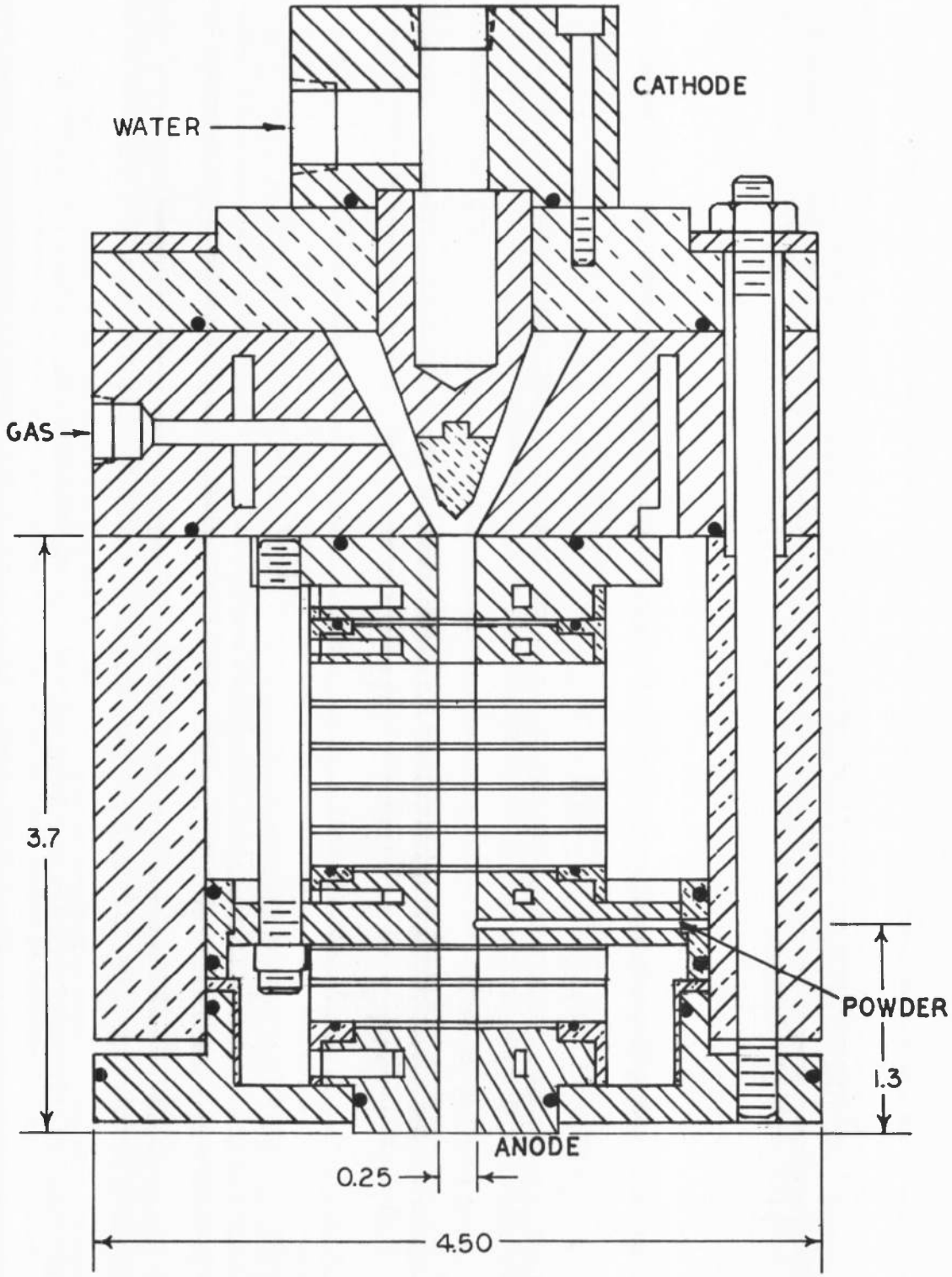

Fig. 4. Schematic diagram of first plasma jet configuration.

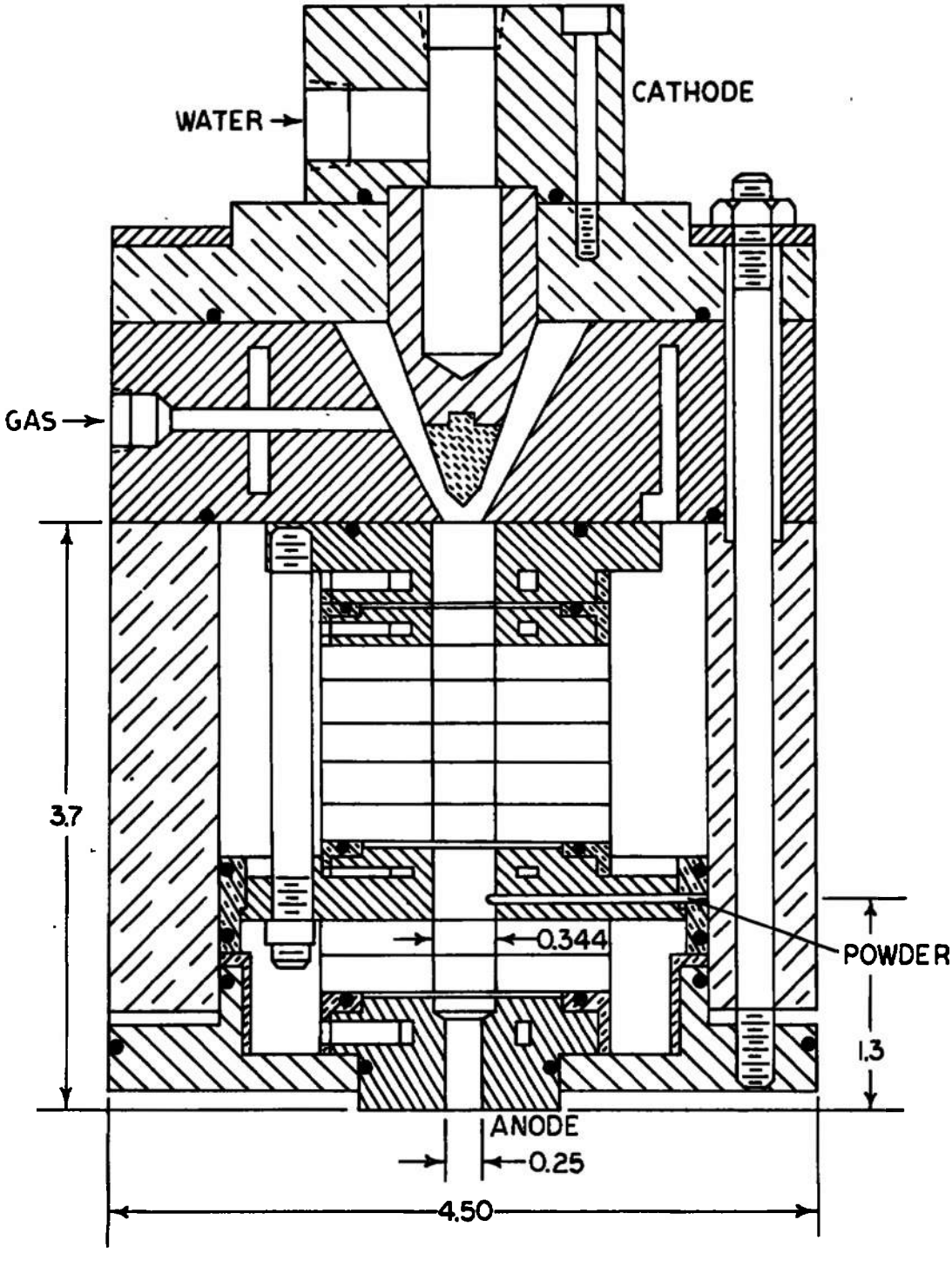

Fig. 5. Schematic diagram of second plasma jet configuration

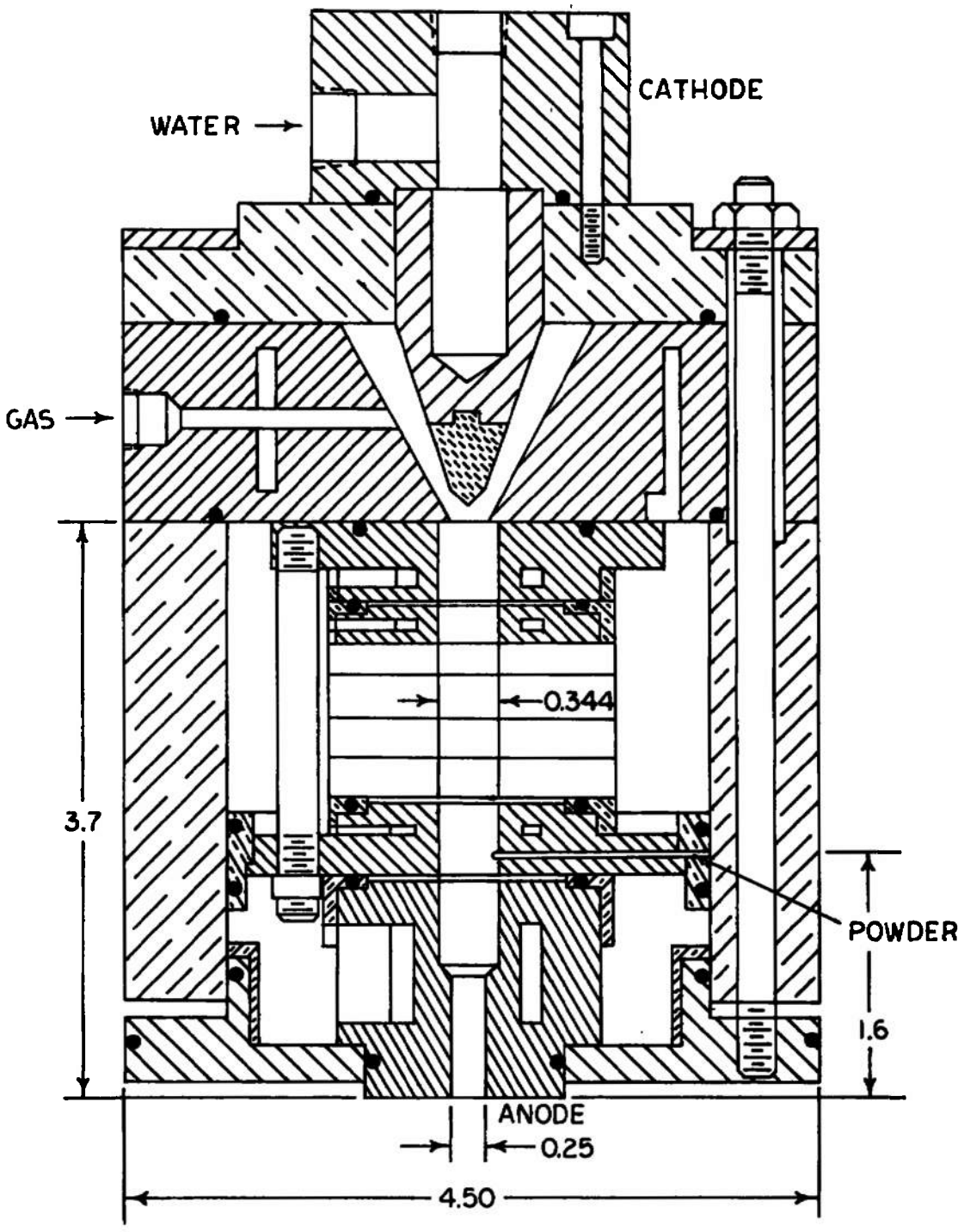

Fig. 6. Schematic diagram of third plasma jet configuration.

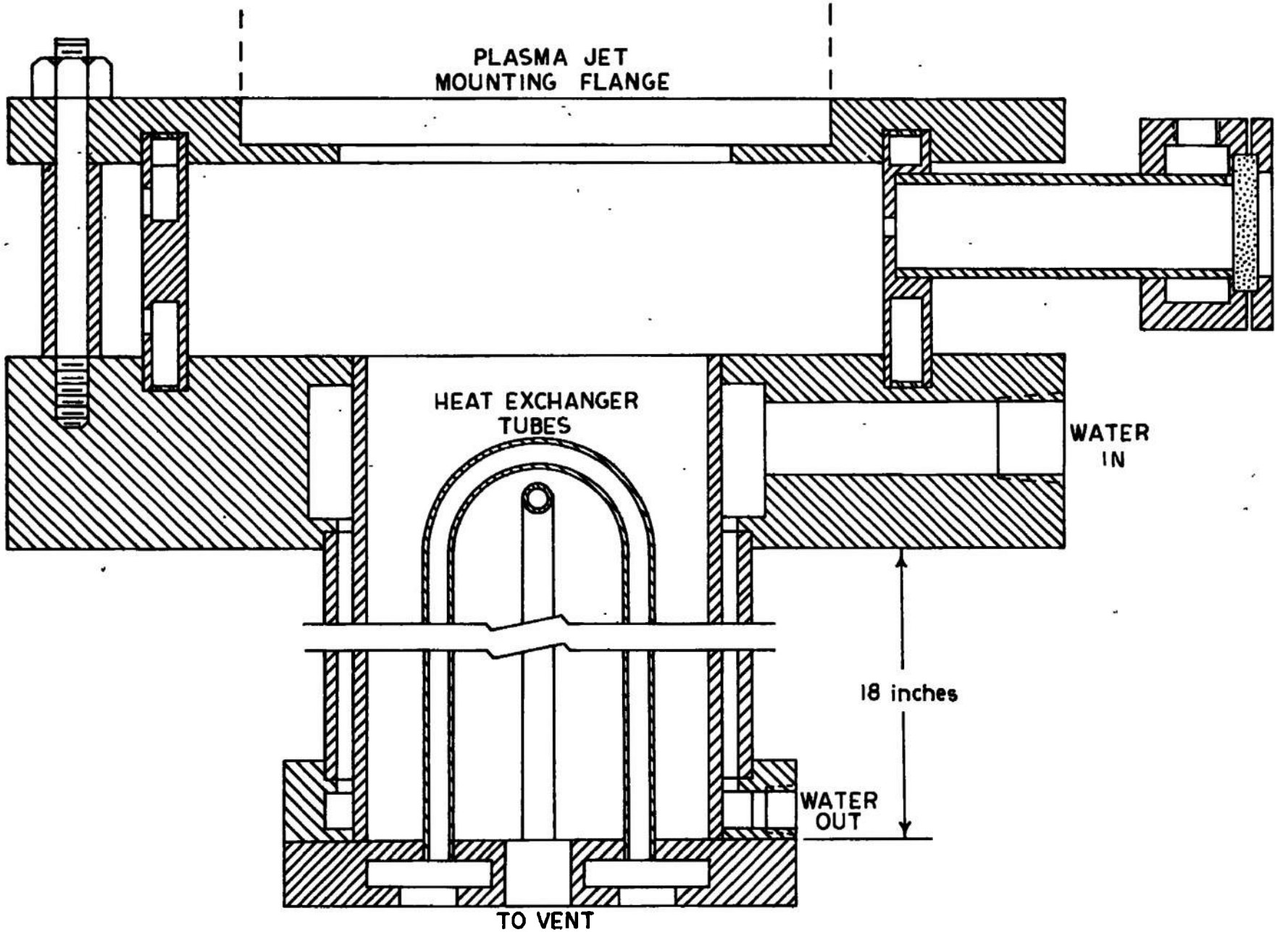

Fig. 7. Schematic diagram of observation plenum chamber and quench chamber.

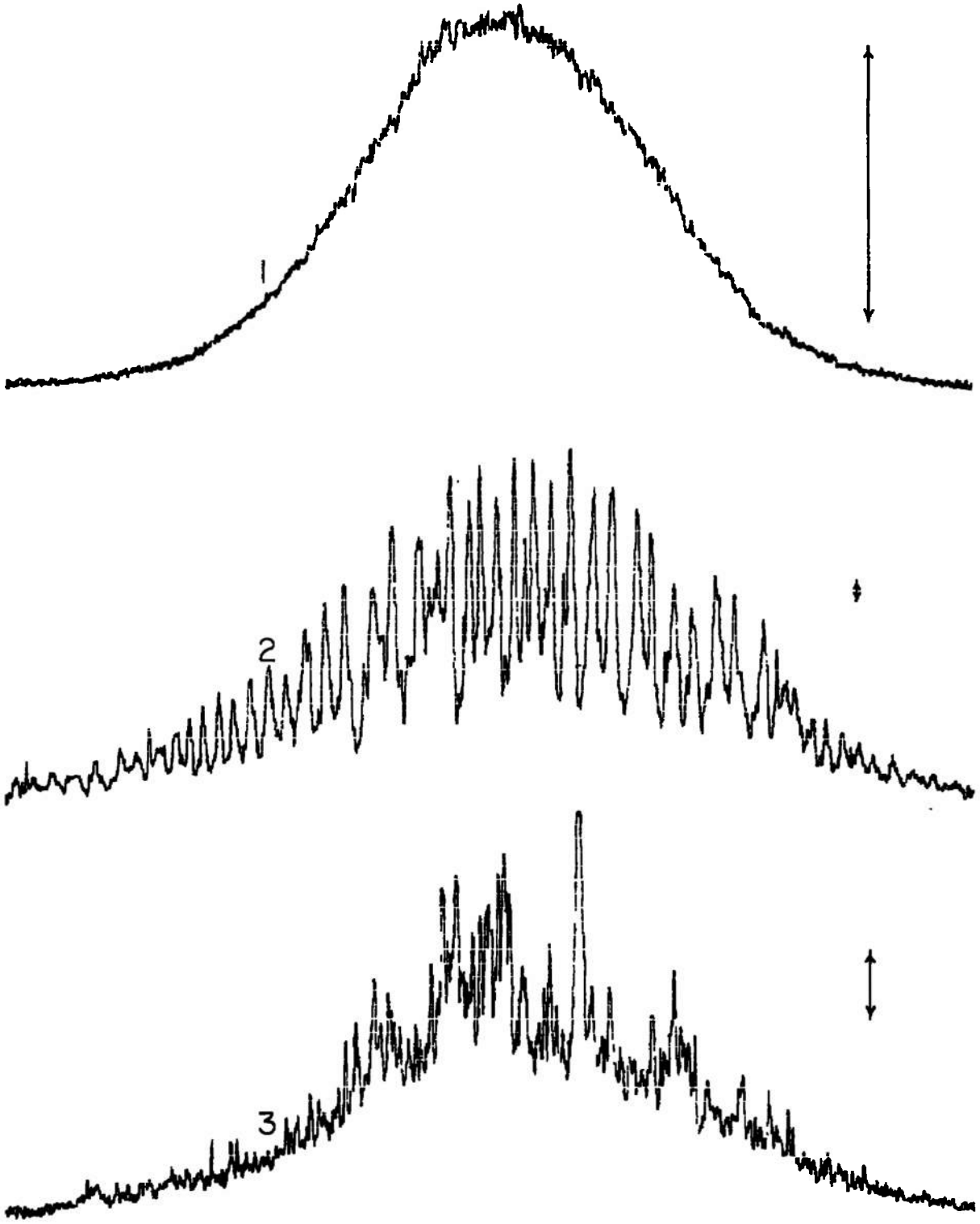

Fig. 8. Sample recorder traces of continuum intensity showing the stability of the unseeded jet (1), the pulsing nature of Metco feeder without the fluidizer (2), and the improvement resulting from the fluidizer (3), where the arrows indicate equivalent fluctuations.

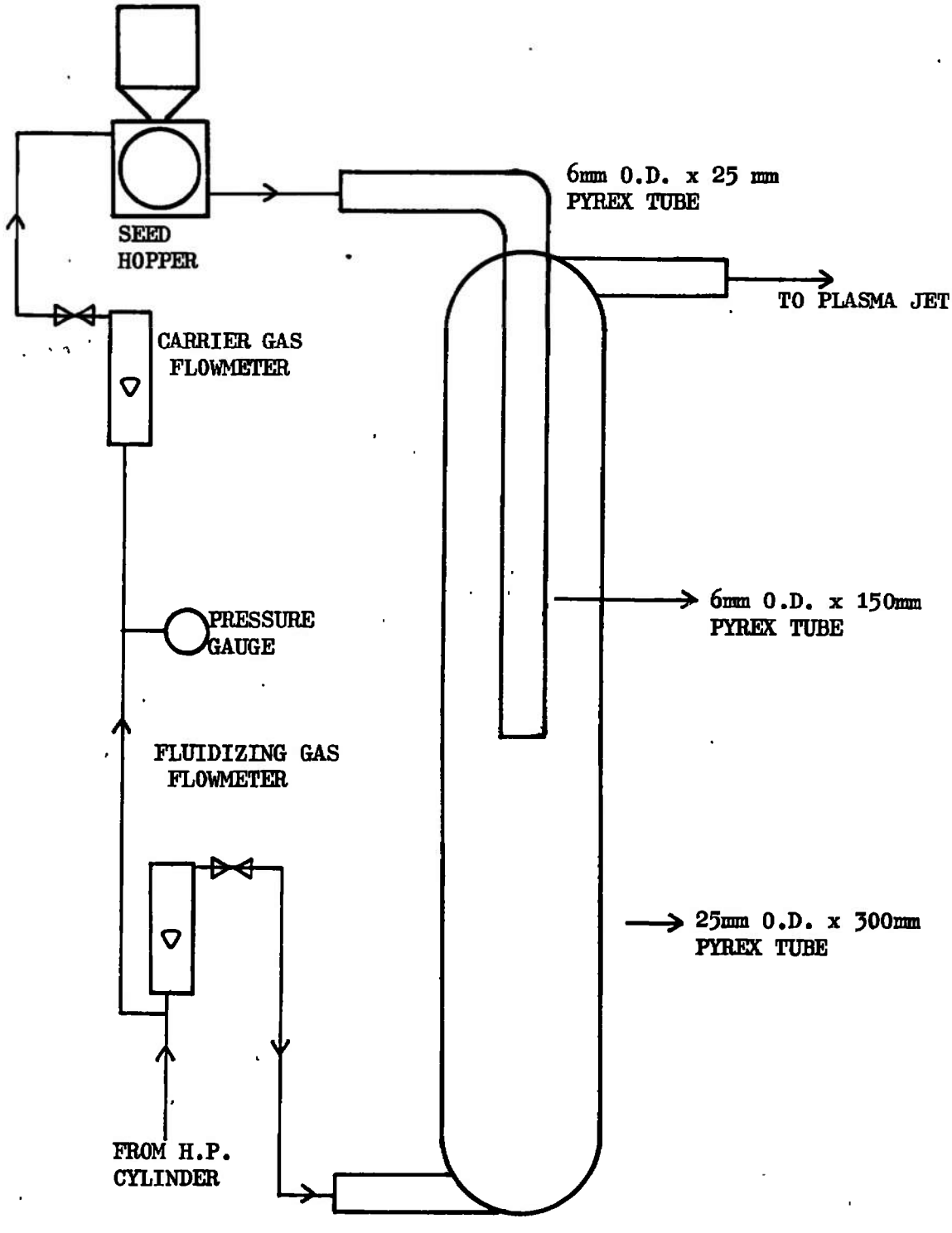

Fig. 9. Schematic diagram of fluidizer used to improve the uniformity of seed distribution.

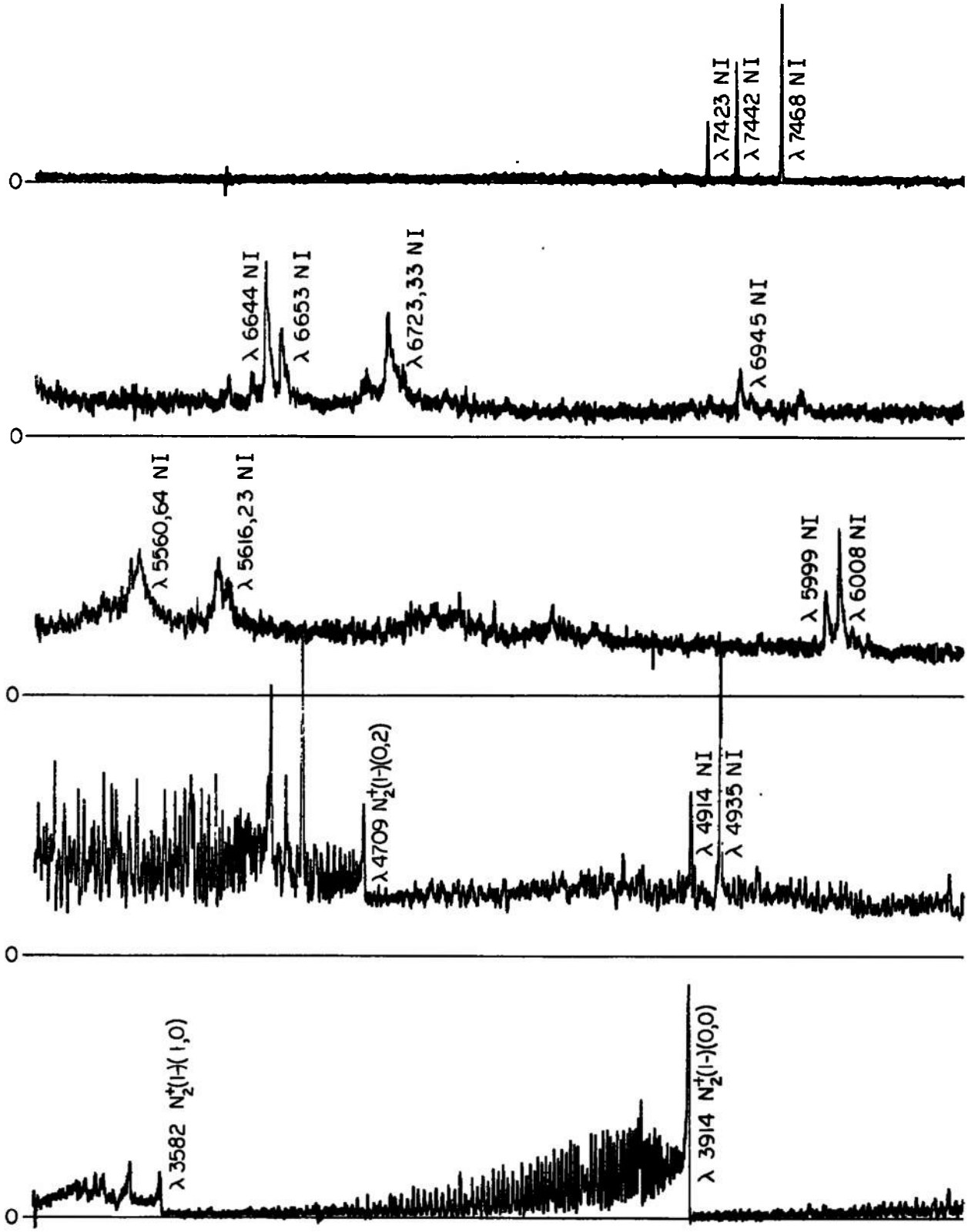

Fig. 10. Sample wavelength traces of the integrated intensity spectrum emitted along central ray of pure nitrogen jet of first configuration.

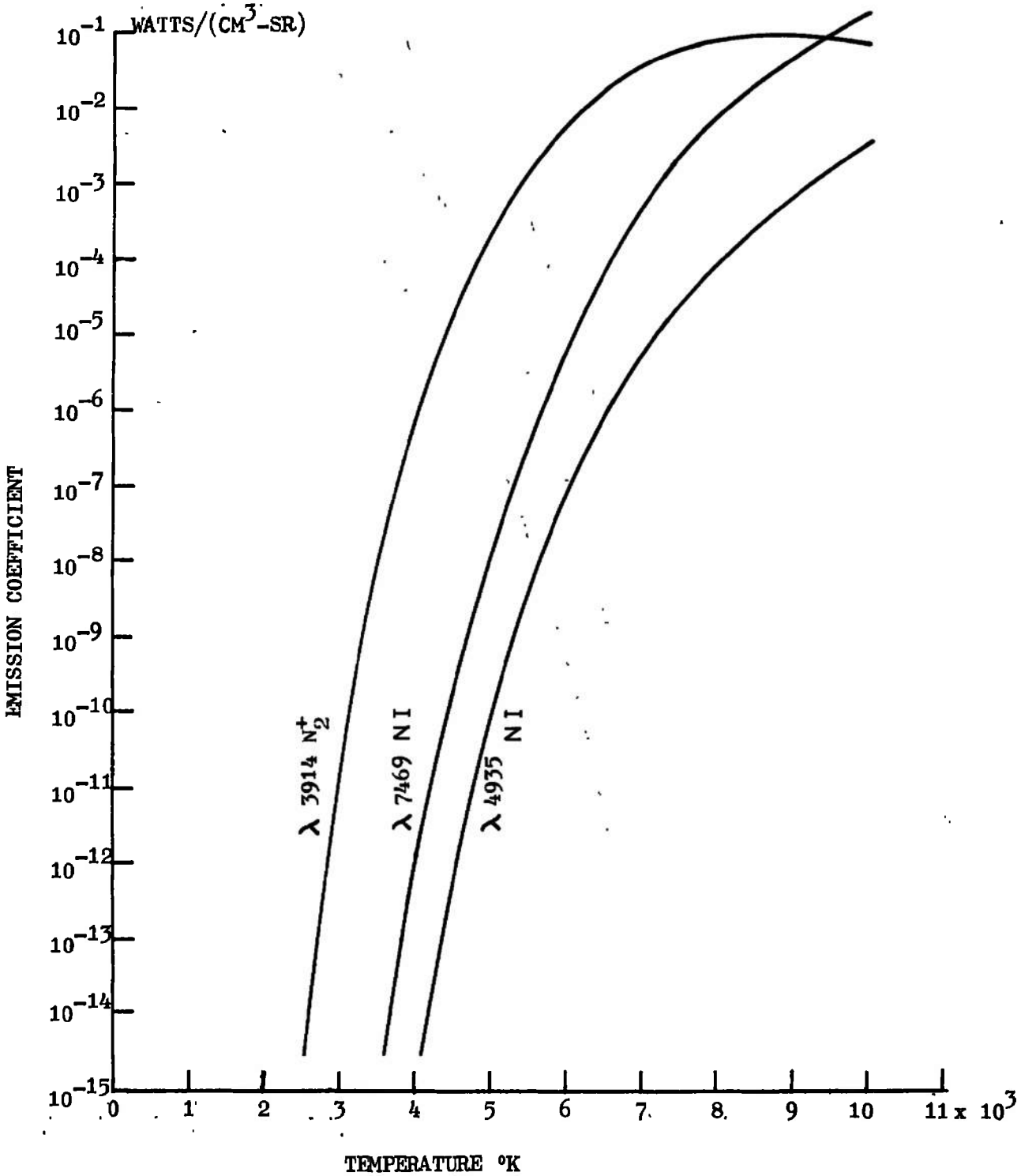

Fig. 11. Emission coefficient vs temperature for λ 7469NI, λ 4935NI and λ 3914 $N_2^+(1-)(0,0)$ band increment, δλ, for unseeded 1 atm N_2 plasma.

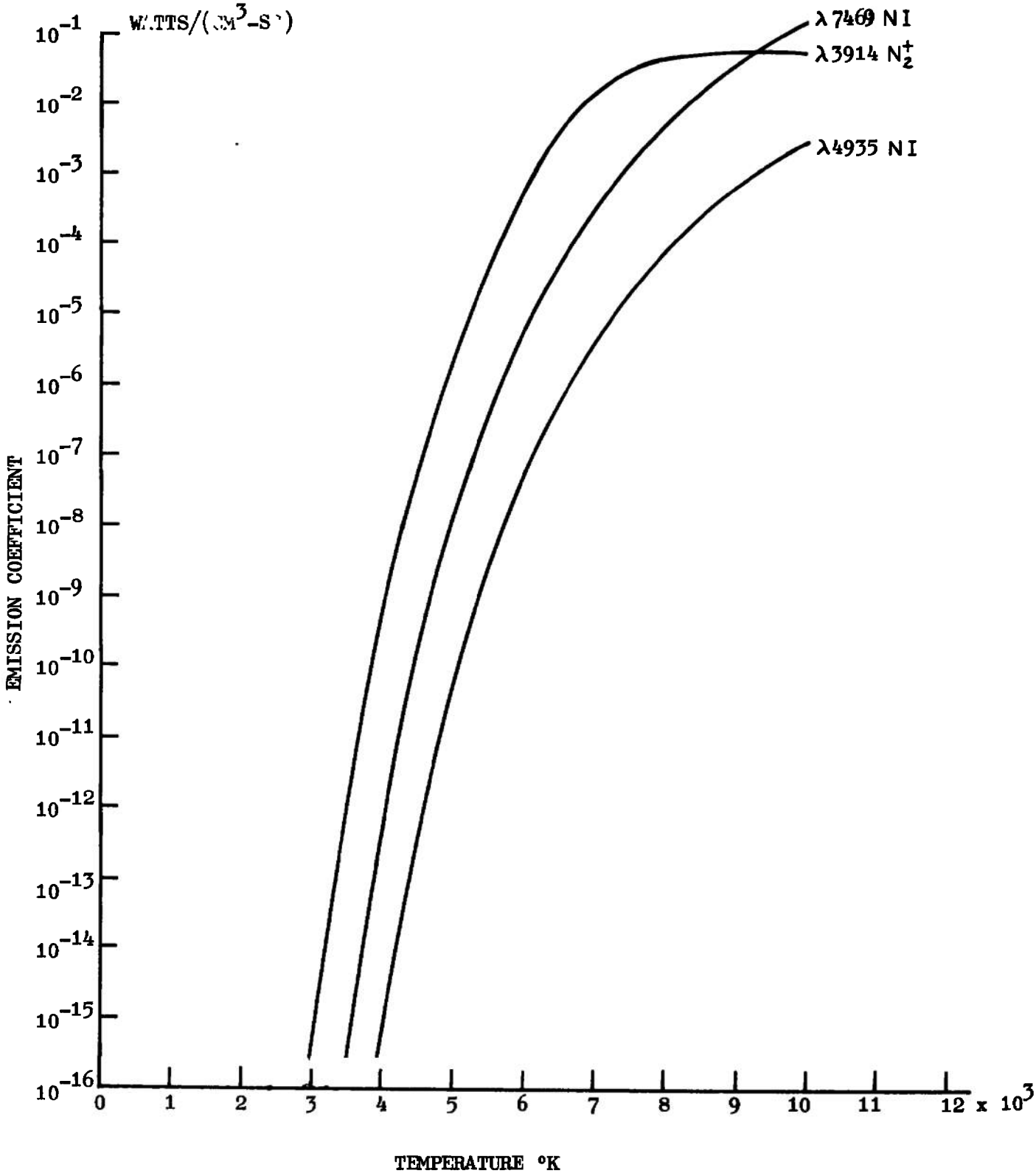

Fig. 12. Emission coefficient vs temperature for λ 7469NI, λ 4935 NI and λ 3914 $N_2^+(1-)(0,0)$ band increment, δλ, for unseeded 1 atm air plasma.

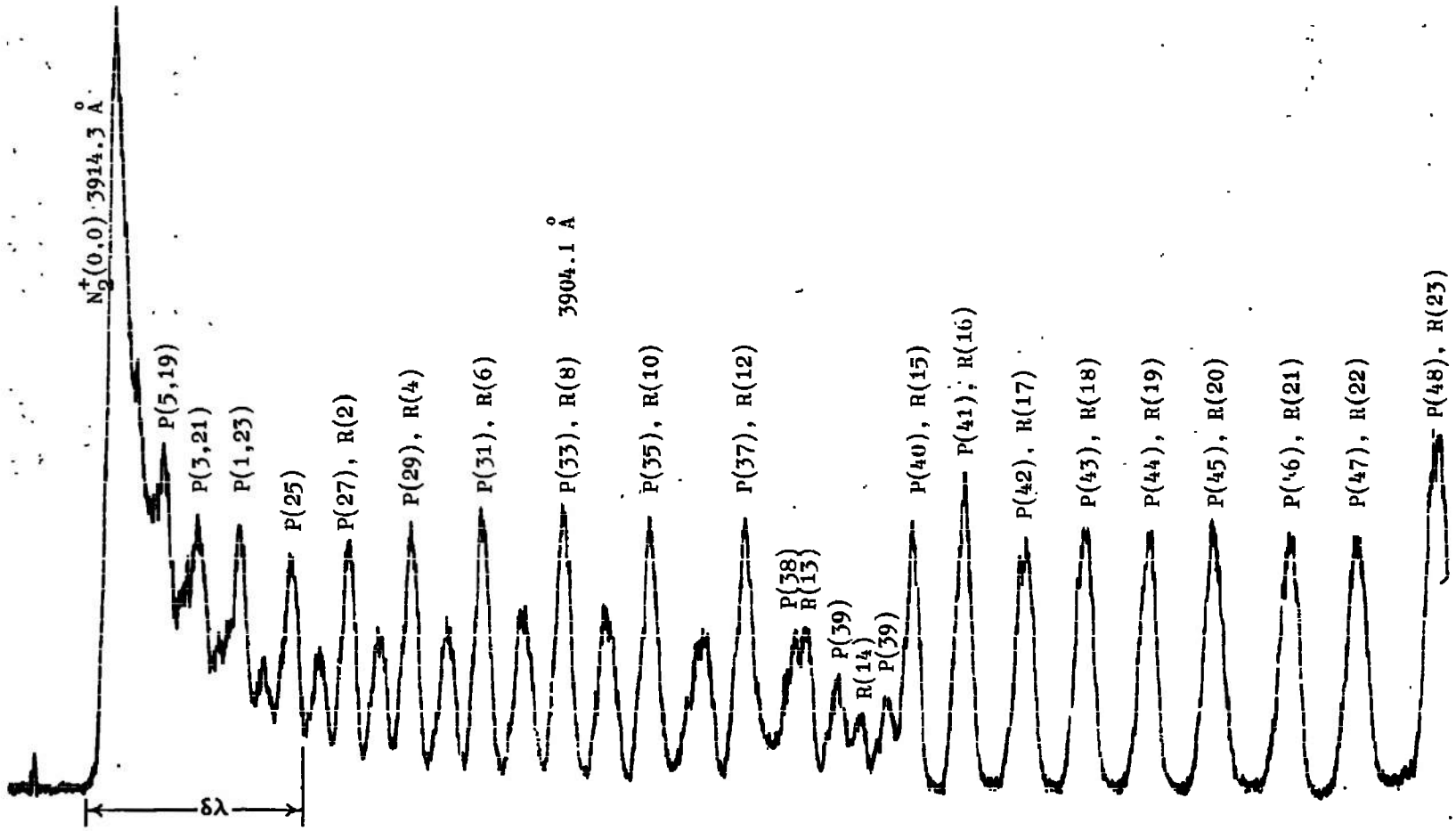

Fig. 13. Observed structure of $N_2^+(1-)(0,0)$ band system in region of band head. Numbers in parenthesis refer to upper K' quantum numbers.

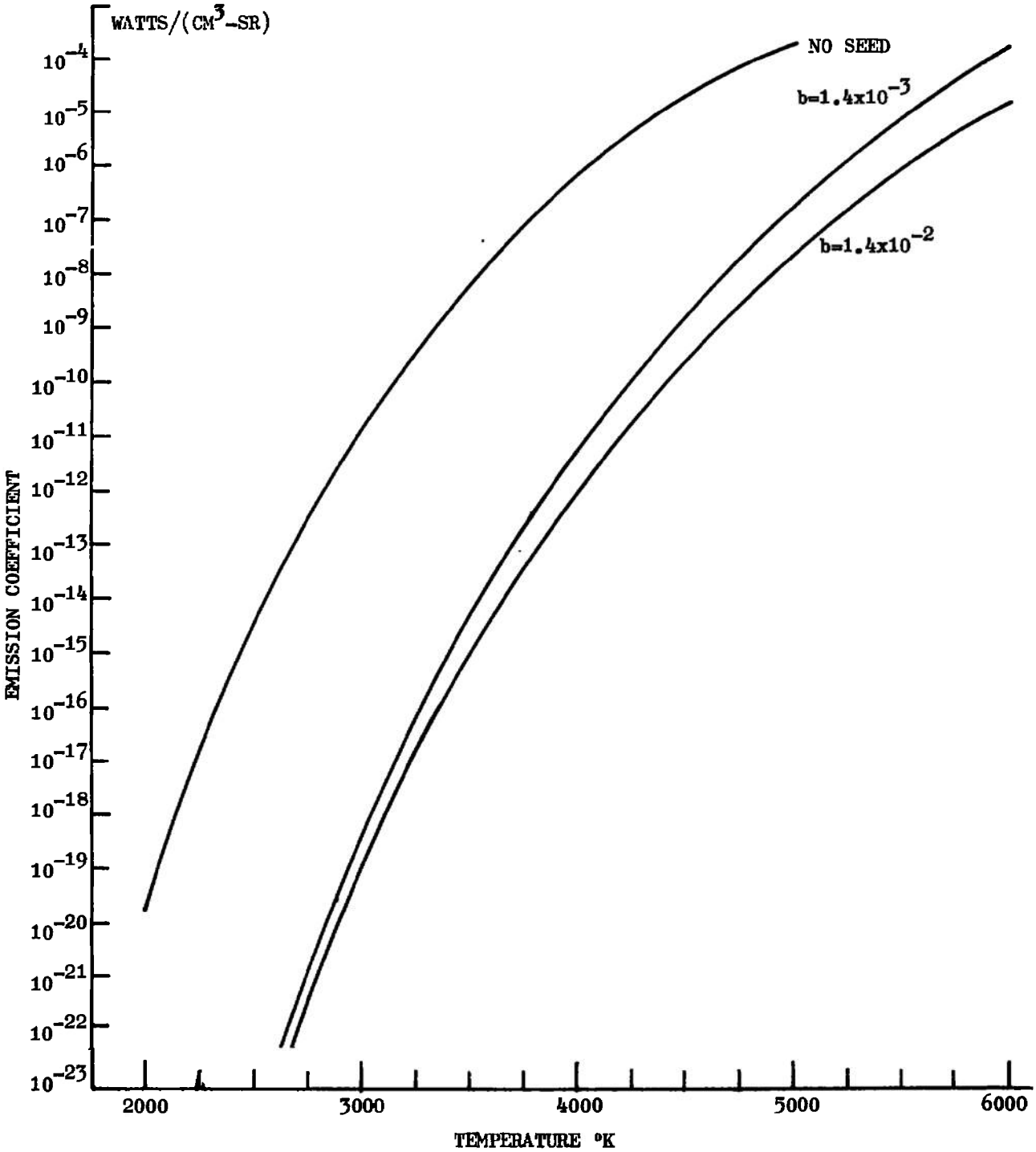

Fig. 14. Emission coefficient of $\delta\lambda$ increment of $N_2^+(1-)(0,0)$ band system vs temperature for 1 atm nitrogen plasma with different seed ratios.

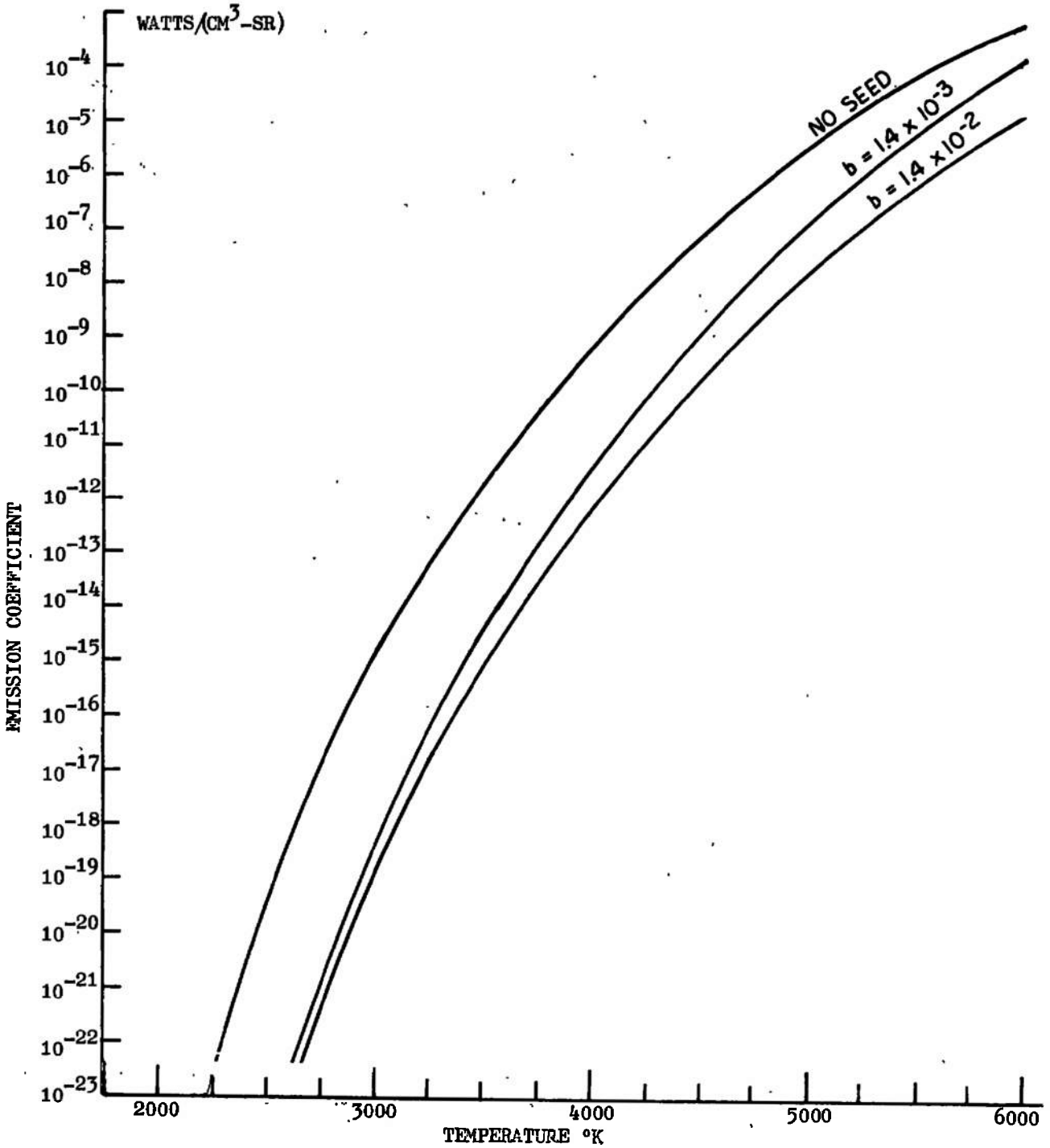

Fig. 15. Emission coefficient of $\delta\lambda$ increment of $N_2^+(1-)(0,0)$ band system vs temperature for 1 atm air plasma with different seed ratios.

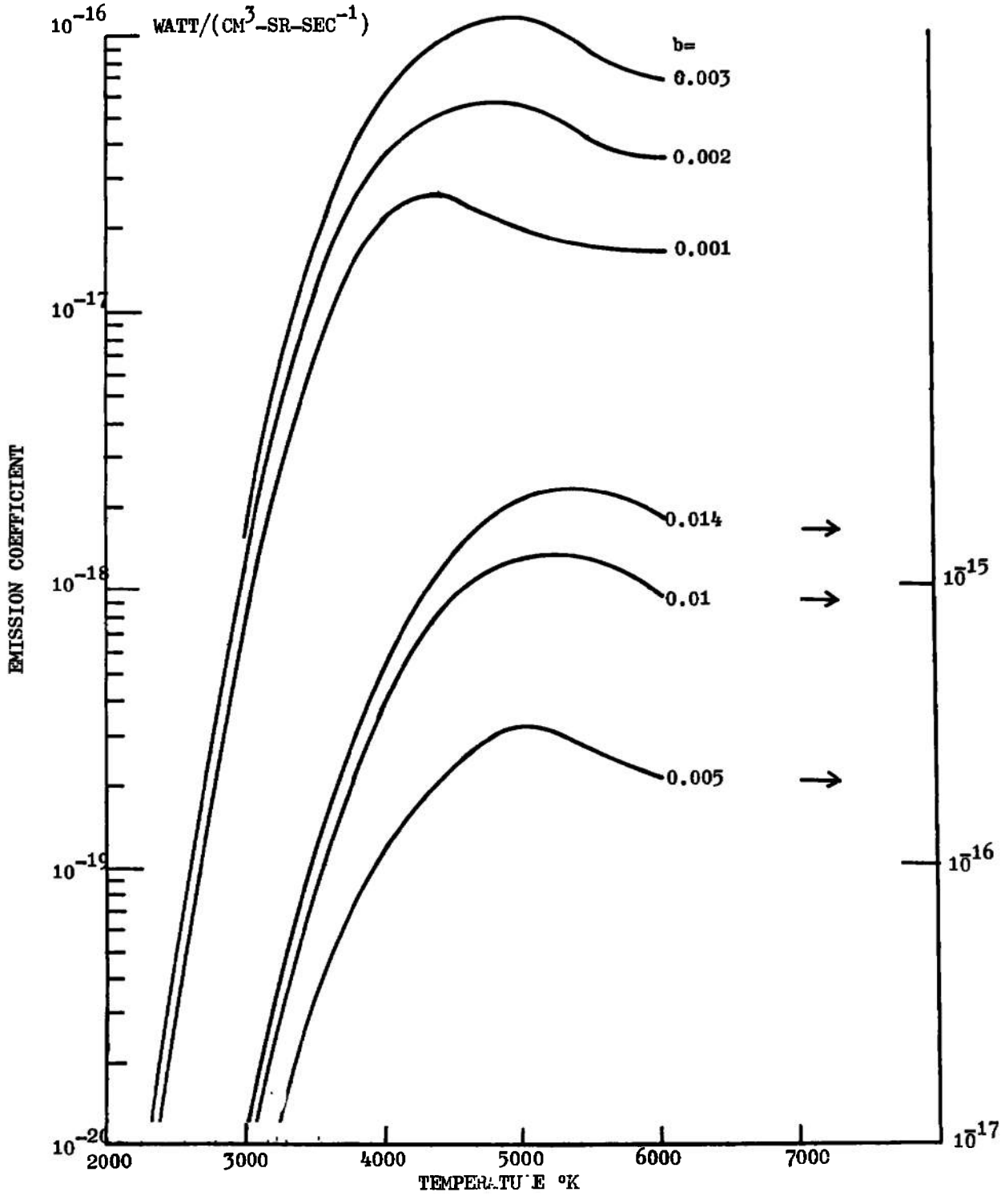

Fig. 16. Emission coefficient of continuum vs temperature for 1 atm nitrogen plasma at different seed ratios. The same curves apply also to the 1 atm air plasma.

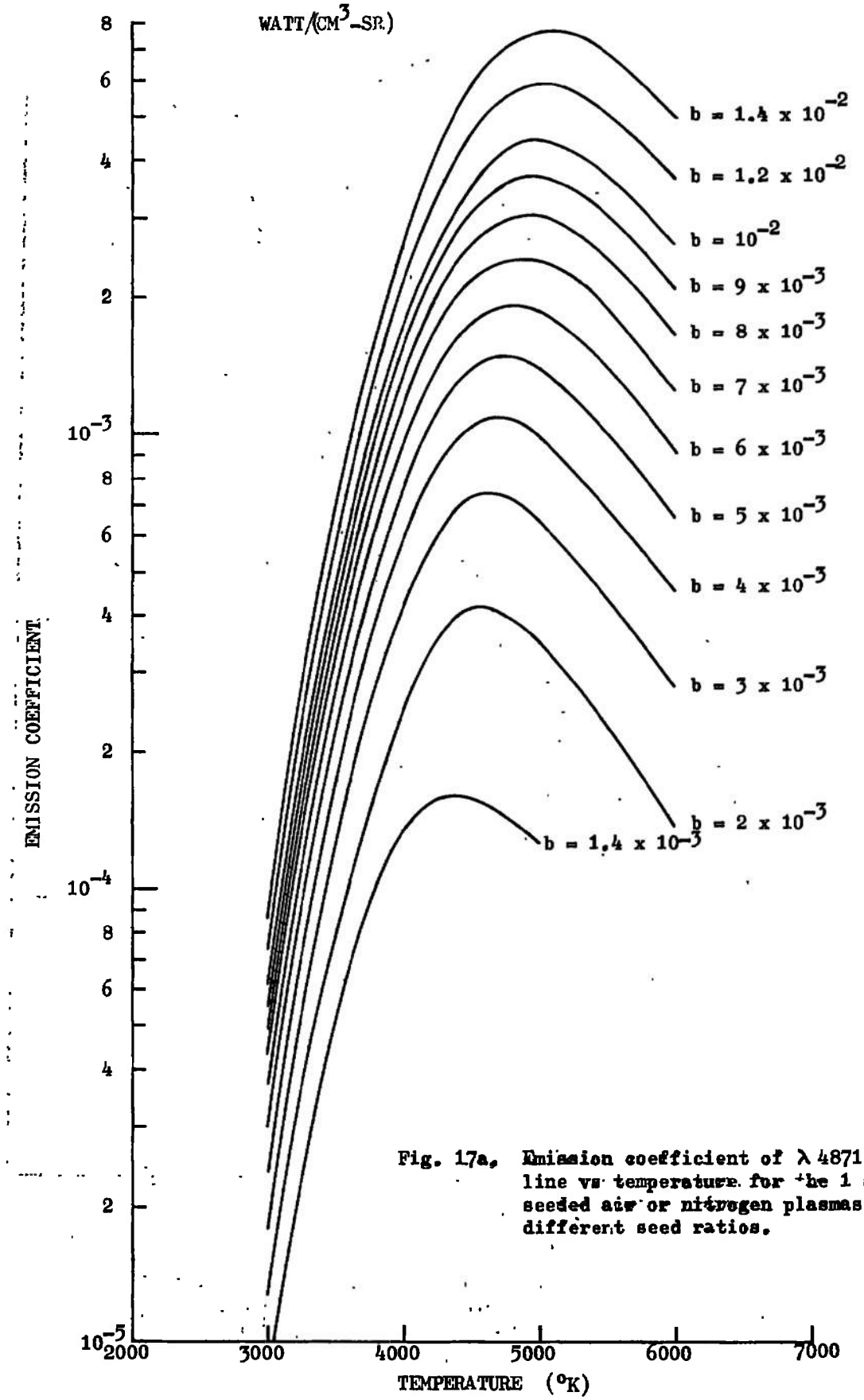

Fig. 17a. Emission coefficient of λ 4871 KI line vs temperature for the 1 atm seeded air or nitrogen plasmas for different seed ratios.

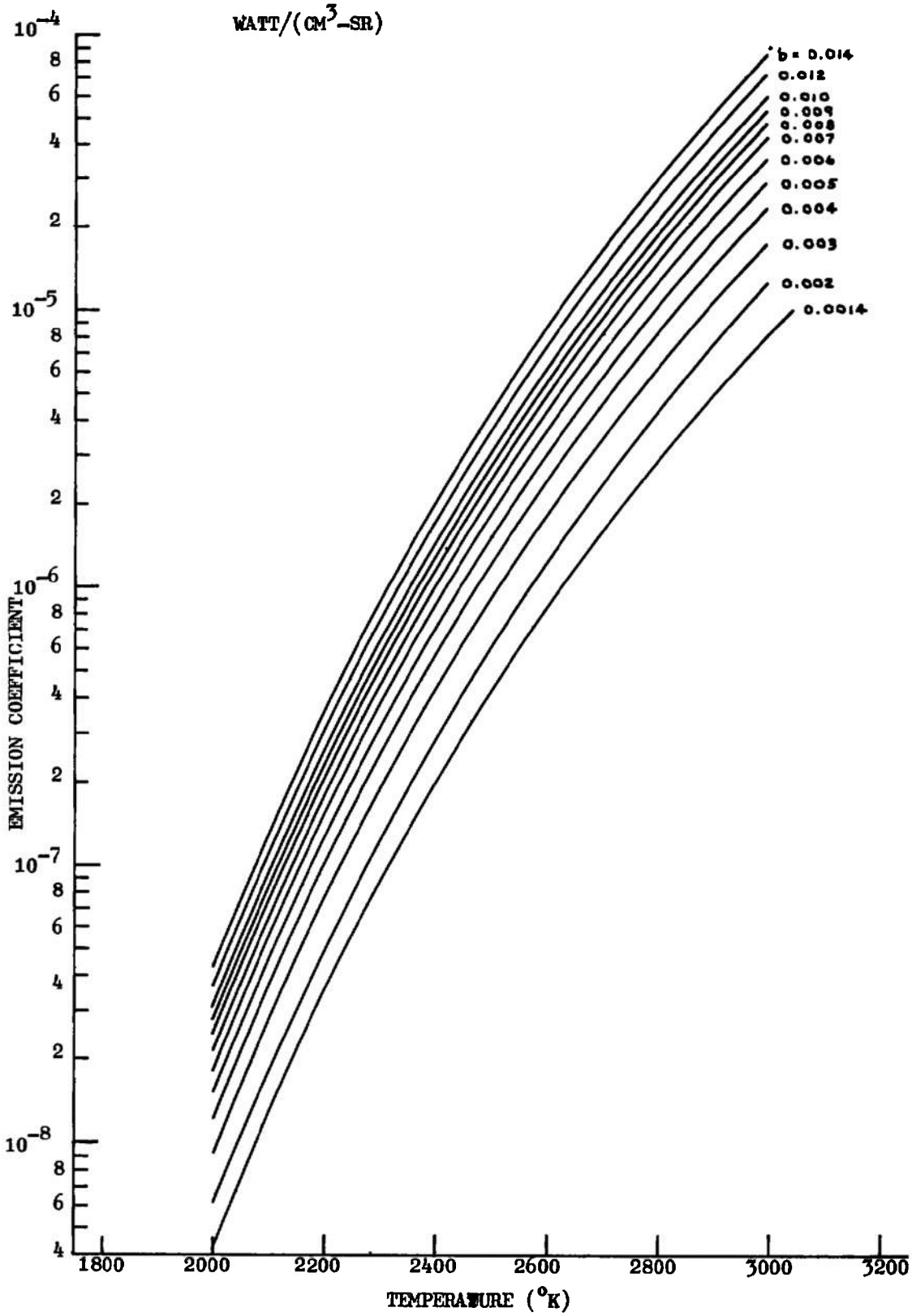

Fig. 17b. Emission coefficient of λ 4871 KI line vs temperature for the 1 atm seeded air or nitrogen plasmas for different seed ratios.

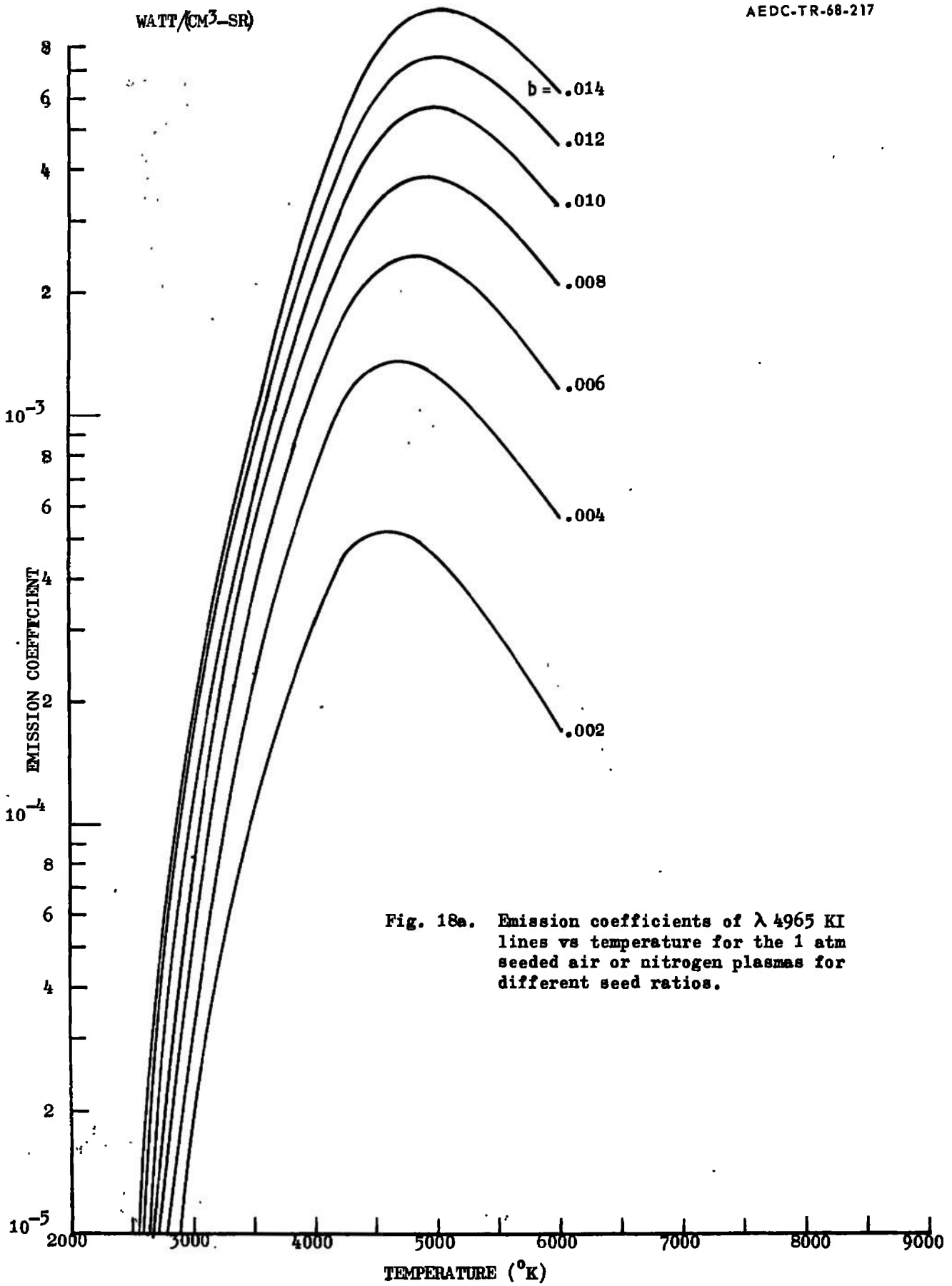

Fig. 18a. Emission coefficients of λ 4965 KI lines vs temperature for the 1 atm seeded air or nitrogen plasmas for different seed ratios.

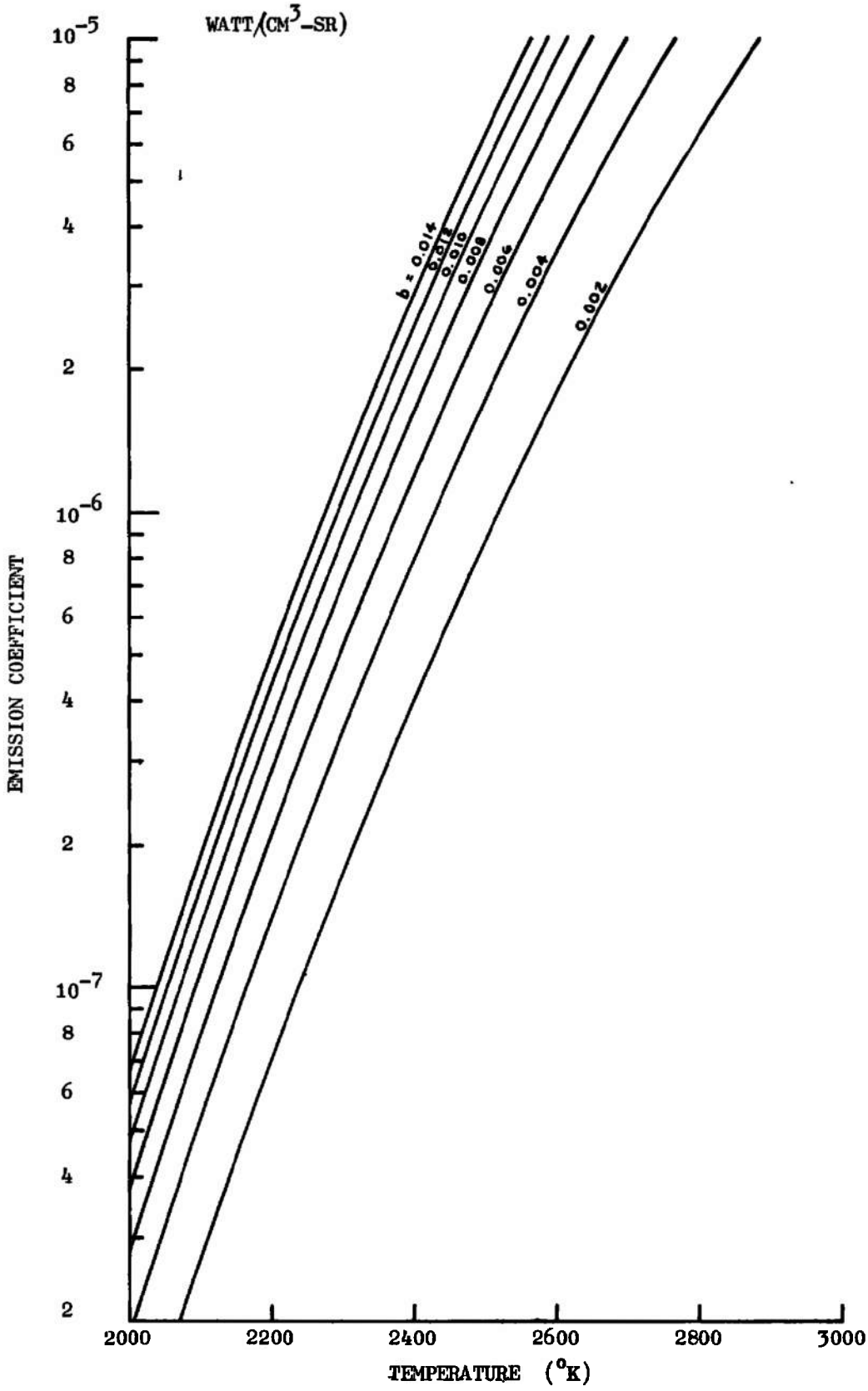

Fig. 18b. Emission coefficients of λ 4965 KI line vs temperature for the 1 atm seeded air or nitrogen plasmas for different seed ratios.

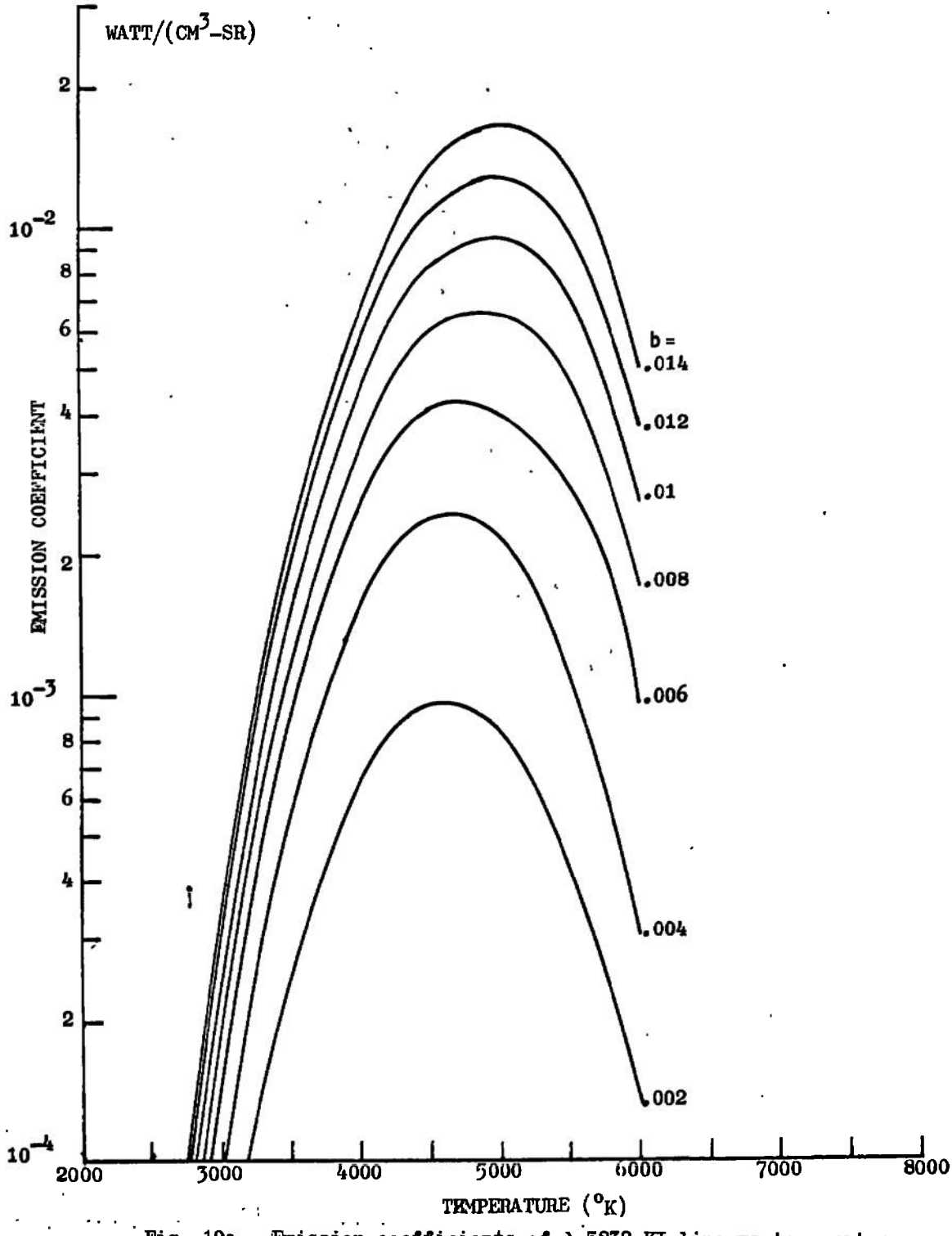

Fig. 19a. Emission coefficients of λ 5832 KI line vs temperature for the 1 atm seeded air or nitrogen plasmas for different seed ratios.

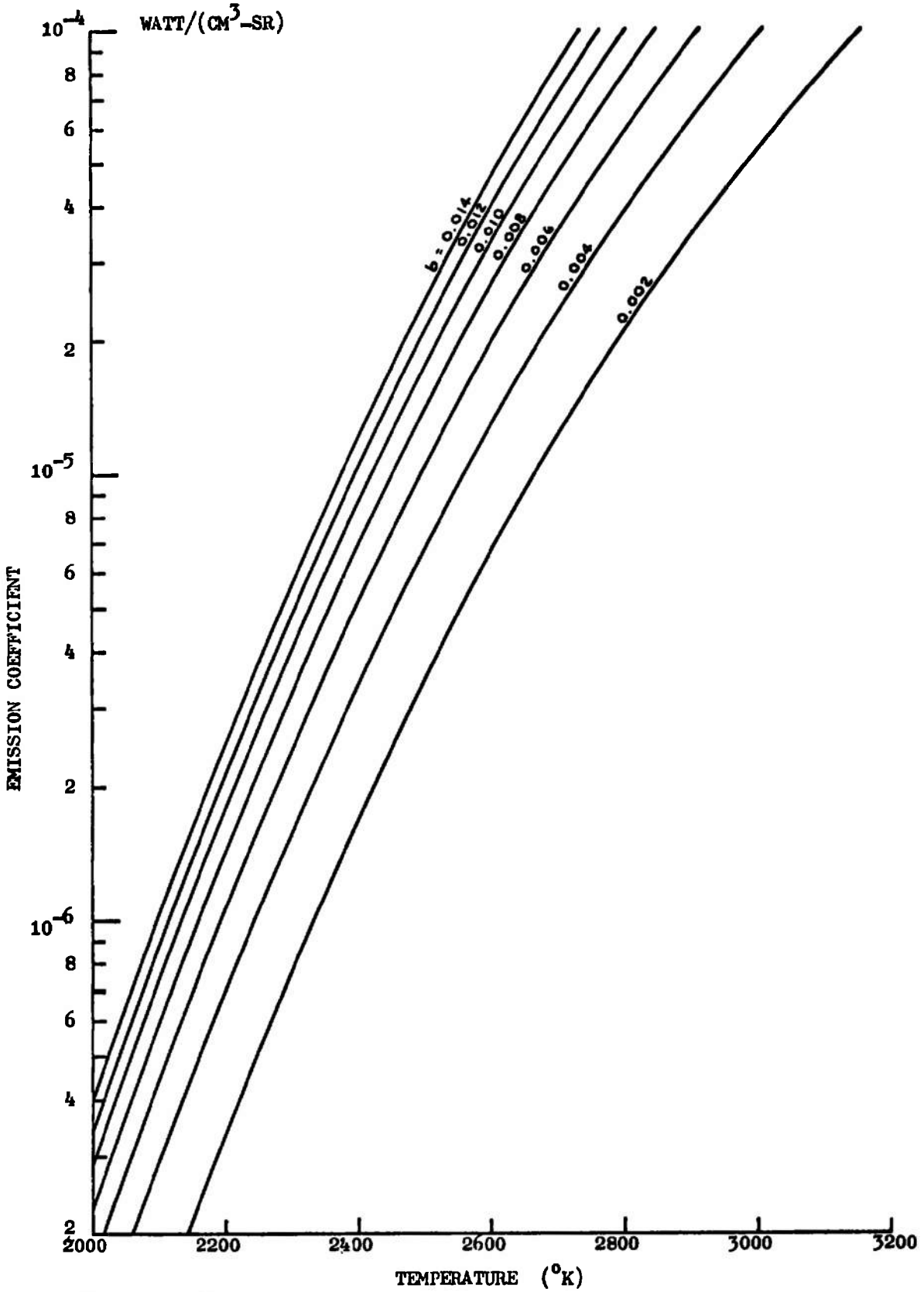

Fig. 19b. Emission coefficients of λ 5832 KI line vs temperature for the 1 atm seeded air or nitrogen plasmas for different seed ratios.

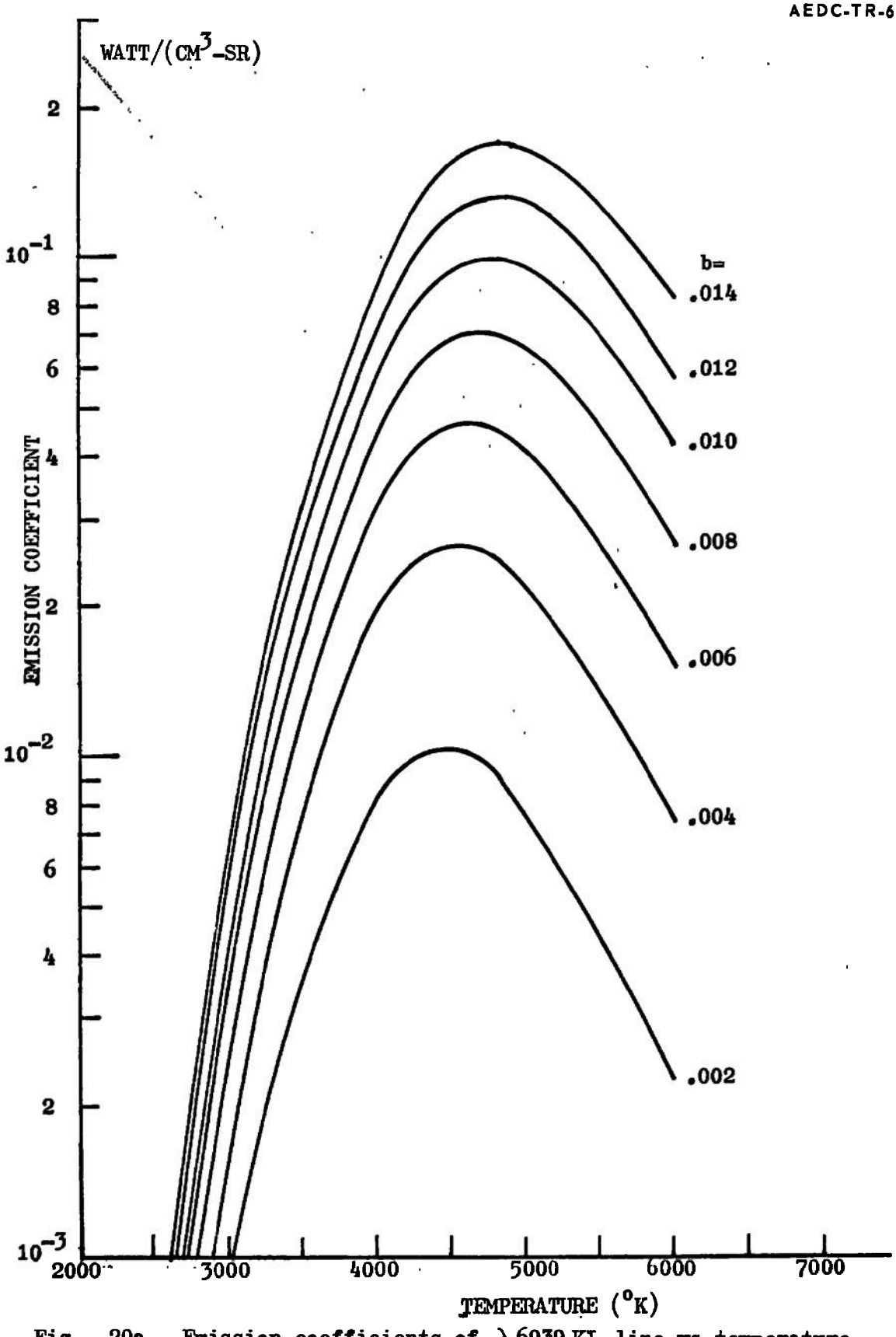

Fig. 20a. Emission coefficients of λ6939 KI line vs temperature for the 1 atm seeded air or nitrogen plasmas for different seed ratios.

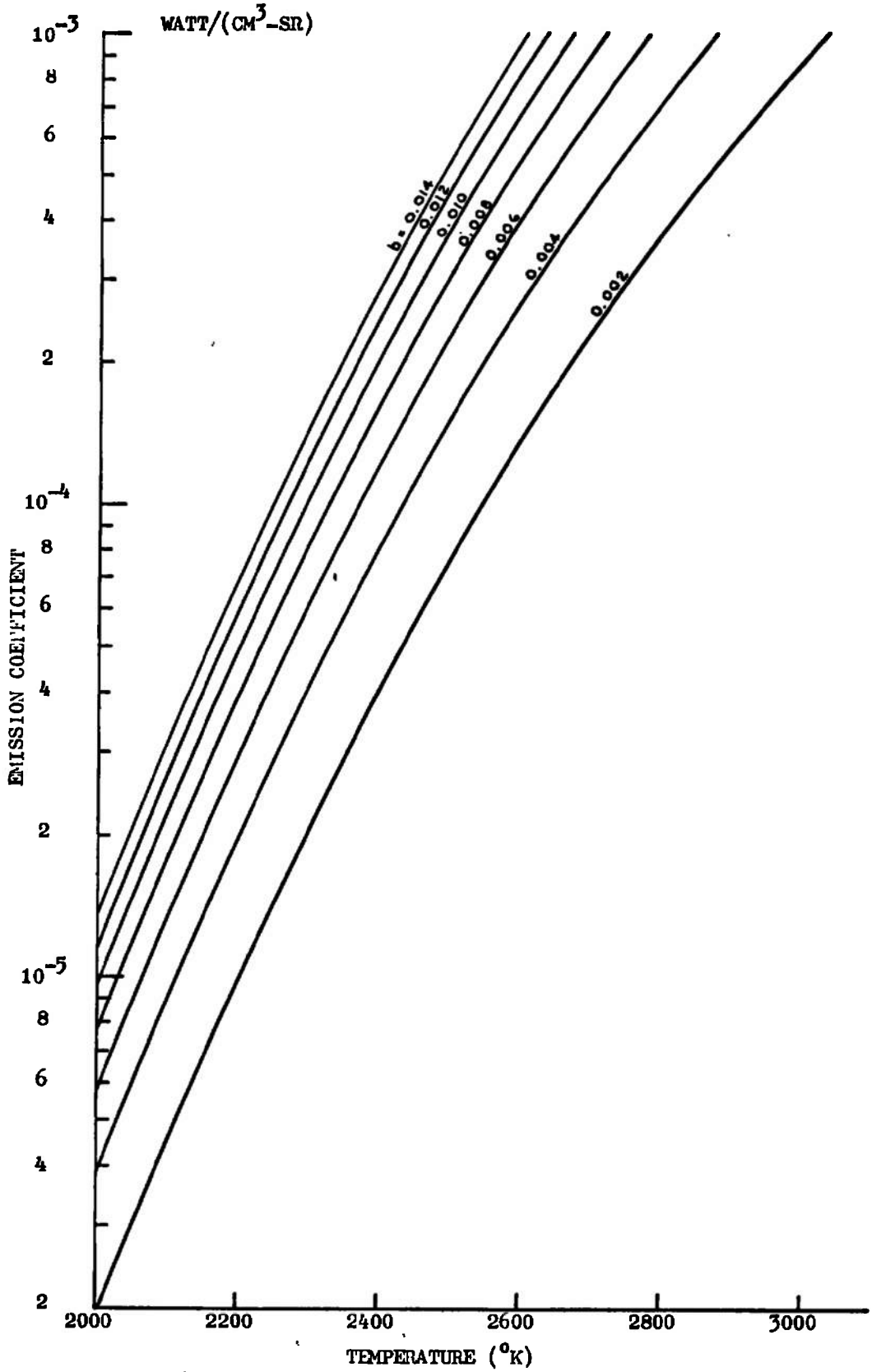

Fig. 20b. Emission coefficients of λ 6939 NI line vs temperature for the 1 atm seeded air or nitrogen plasmas for different seed ratios.

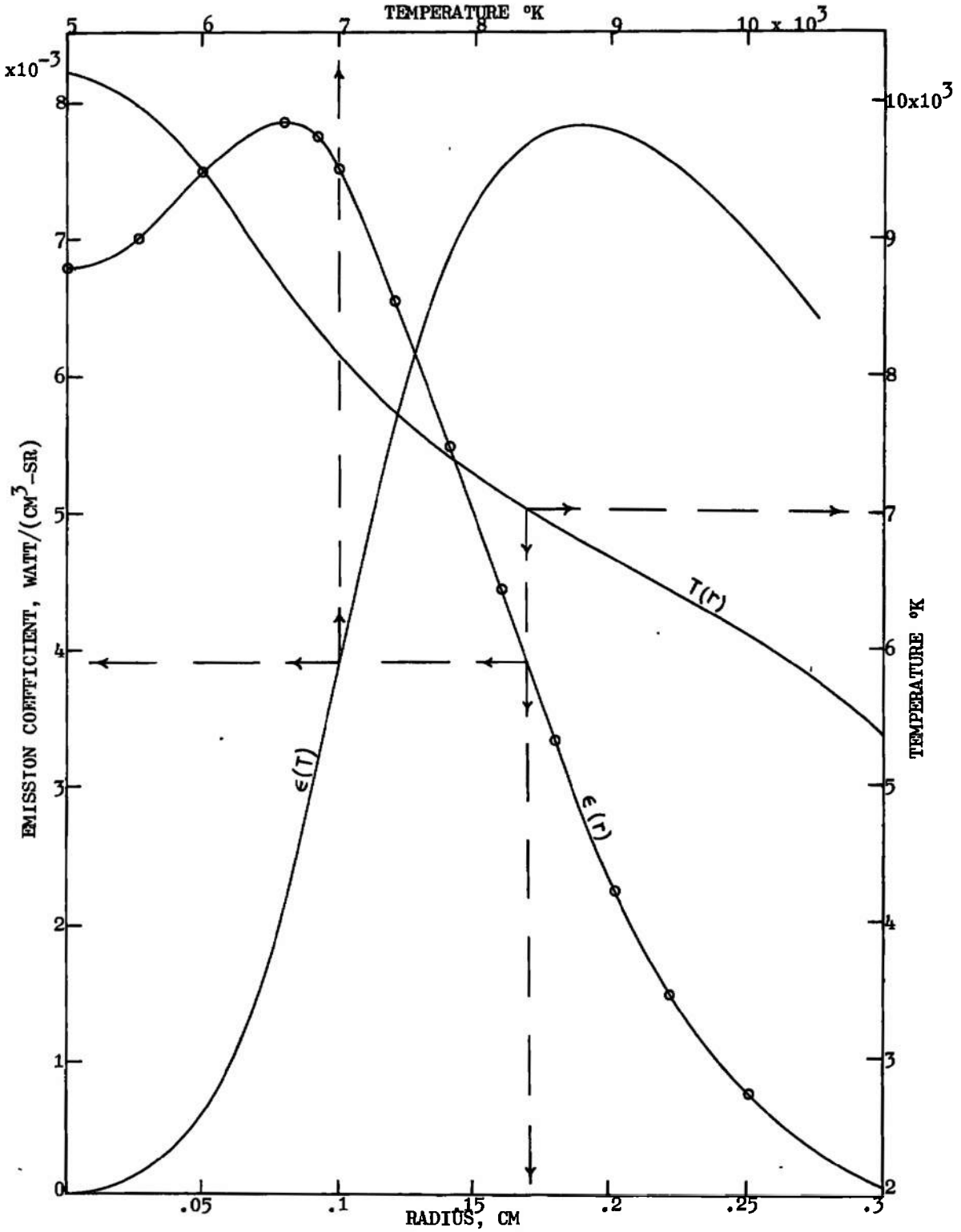

Fig. 21. An illustration of the graphical method used to obtain $T(r)$ from the measured $\epsilon(r)$ and computed $\epsilon(T)$ for the $\delta\lambda$ increment of the λ 3914 $N_2^+(1-)(0,0)$ band for the 1 atm unseeded nitrogen plasma.

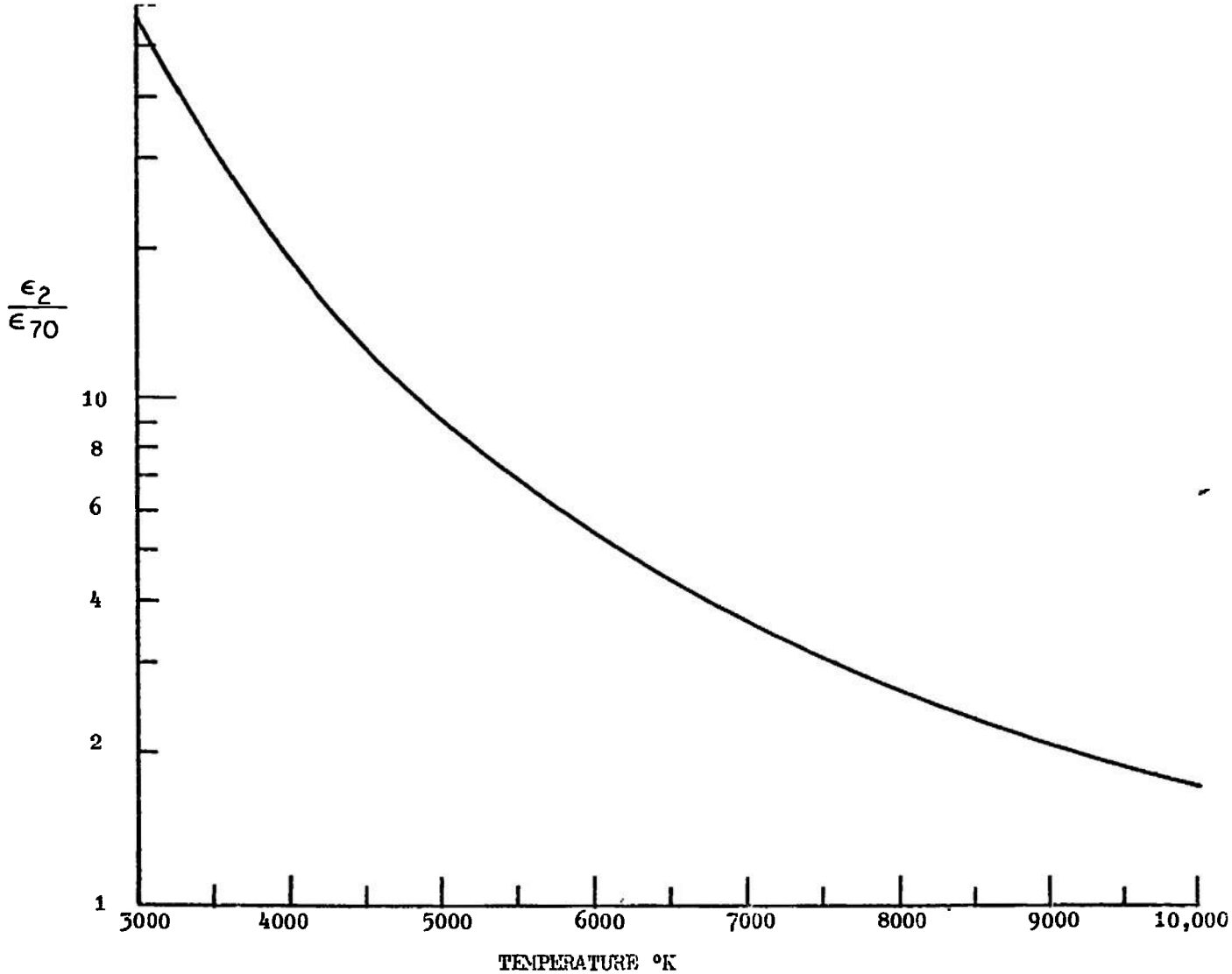

Fig. 22. Temperature dependence of the ratio of emission coefficients for the quartet groupings of rotational components of the $N_2^+(1-)(0,0)$ band system located at the wavelengths of the R branch components having K'=2 and K'=70.

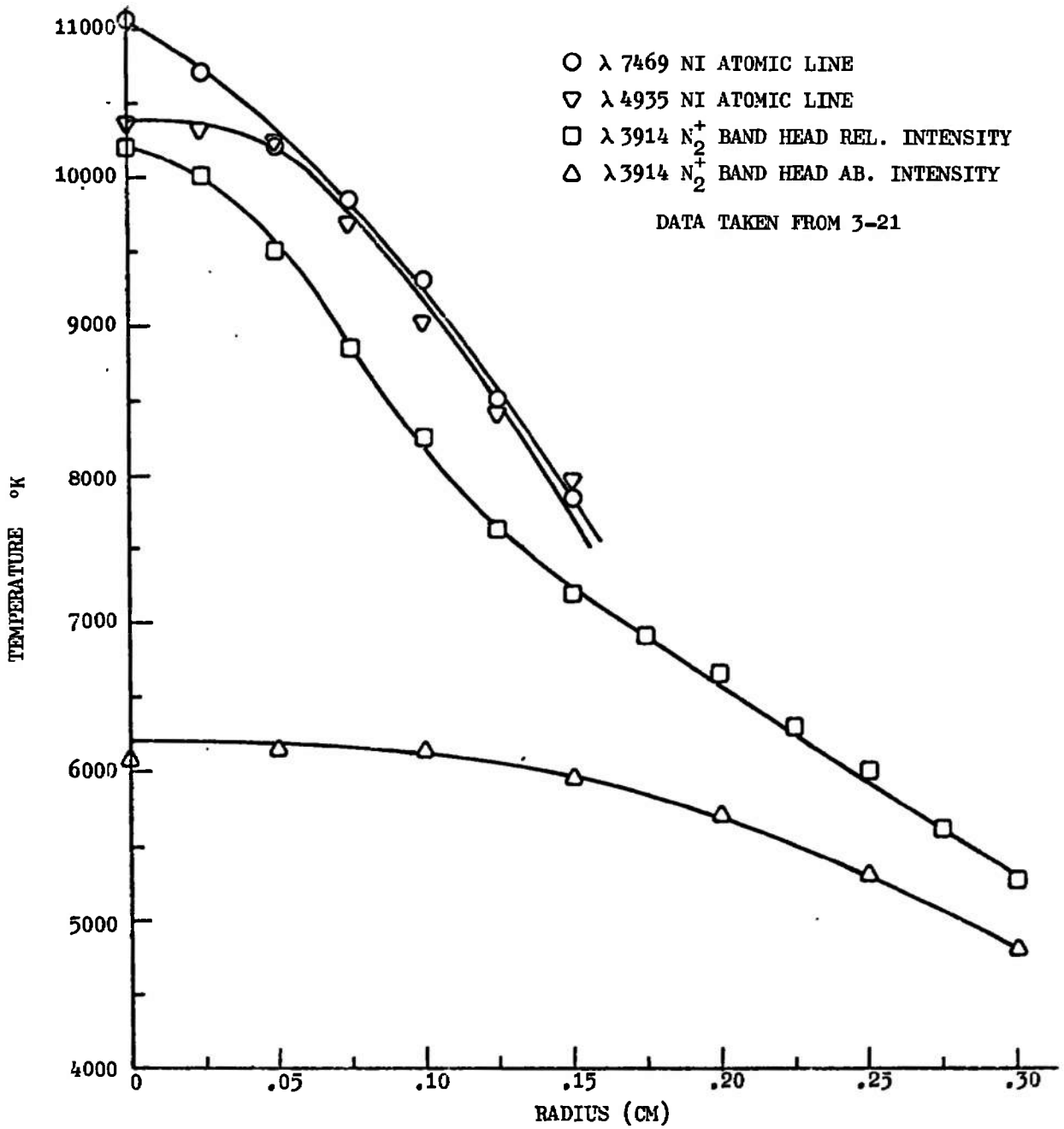

Fig. 23. Comparison of radial temperature profiles determined from various species of radiation emitted by the 1 atm pure nitrogen jet of the second configuration.

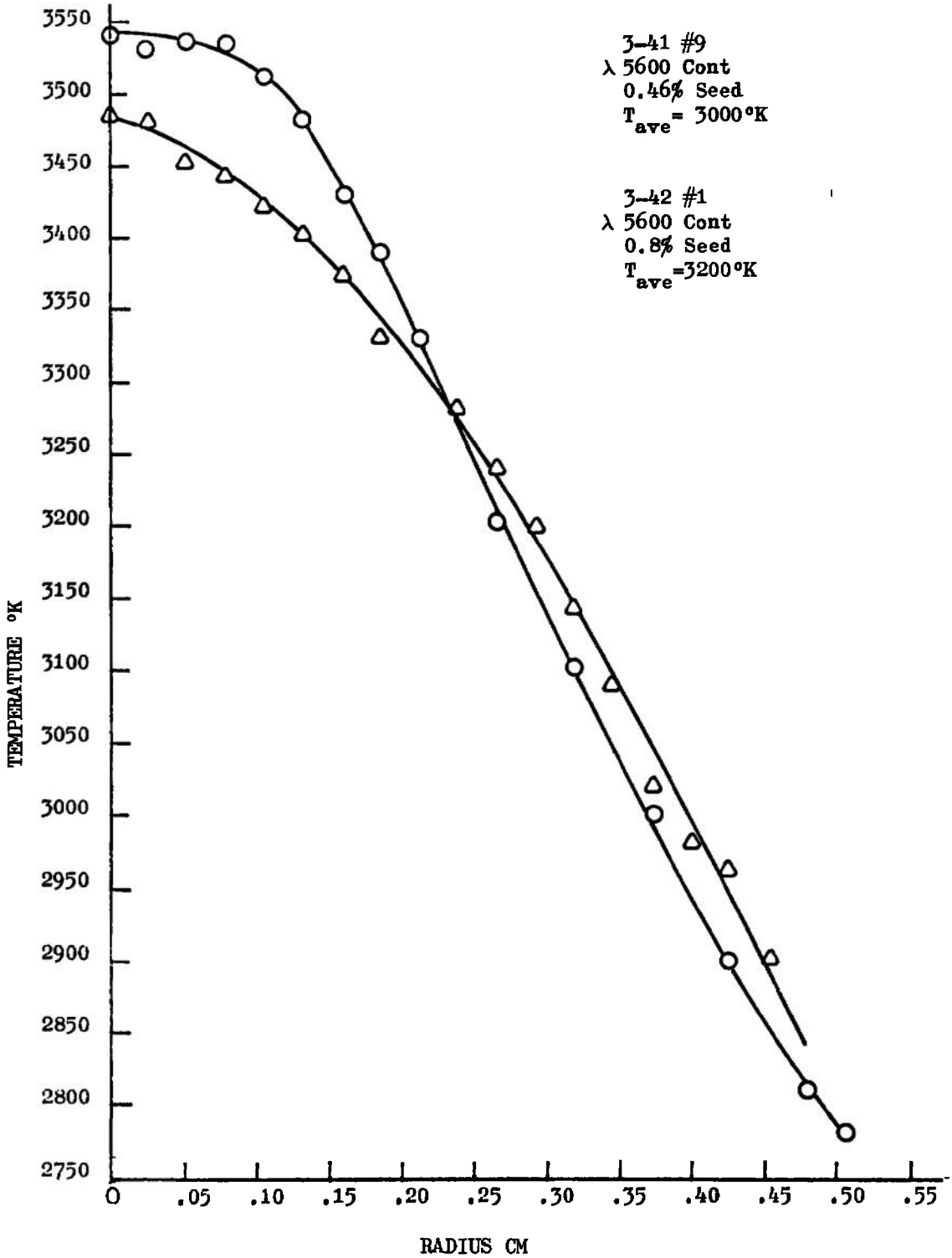

Fig. 24. Radial temperature profiles of the 1 atm seeded air plasma at two seed ratios.

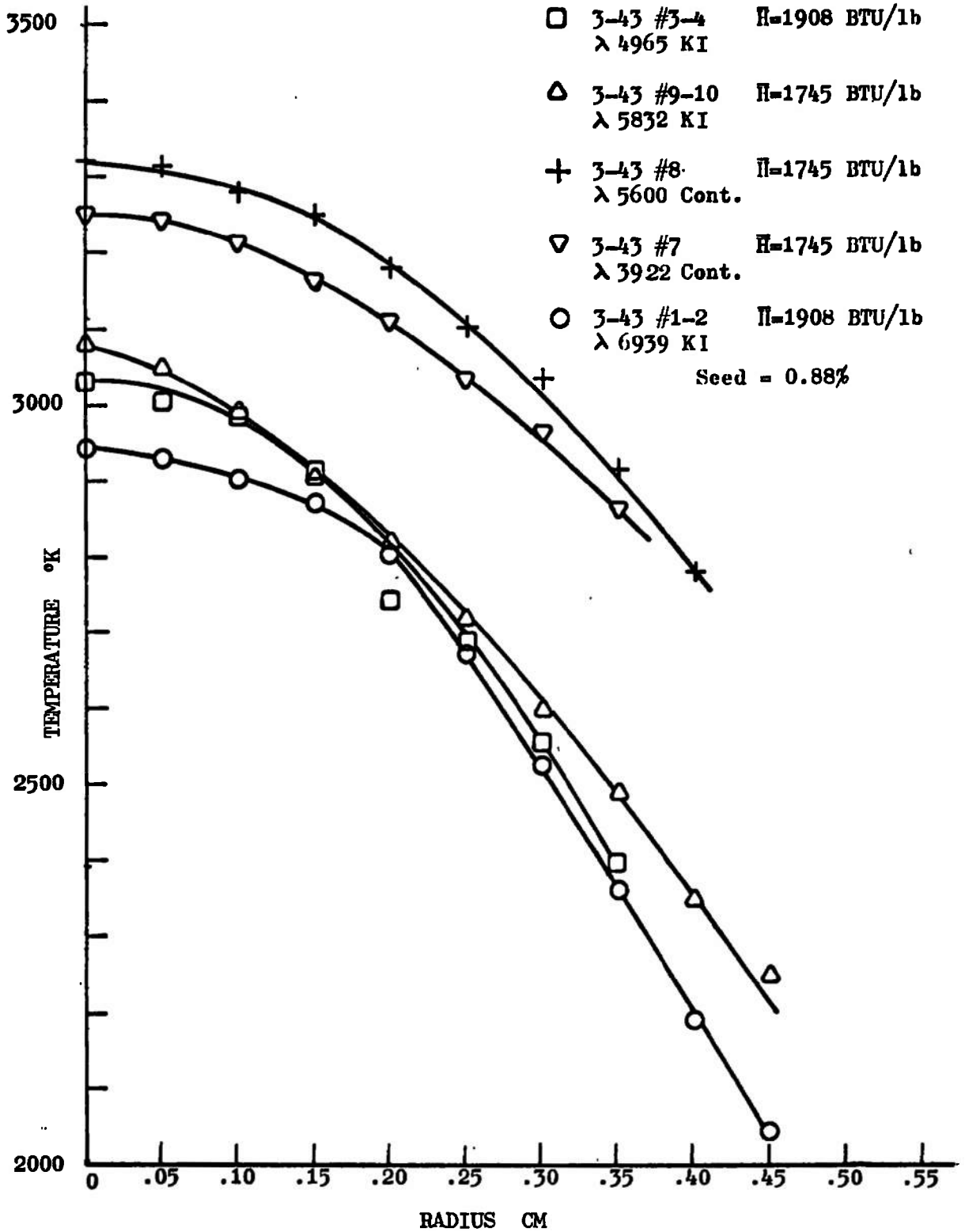

Fig. 25. Radial temperature profiles of the 1 atm .88% seeded air plasma obtained from absolute emission coefficients of five different species of radiation.

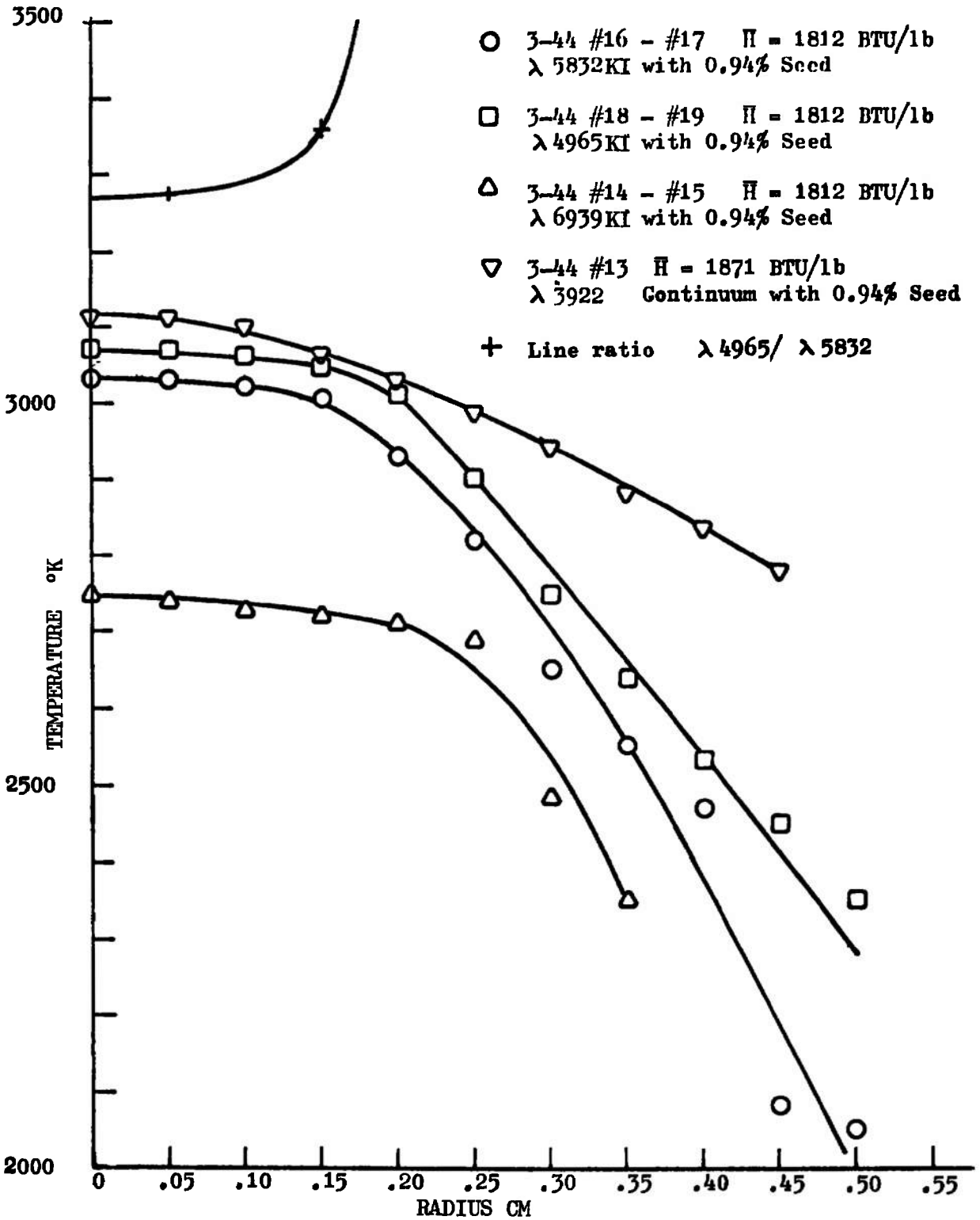

Fig. 26. Radial temperature profiles of the 1 atm .94% seeded air plasma obtained from absolute emission coefficients of four different species of radiation as well as from the ratio of coefficients of two spectral lines.

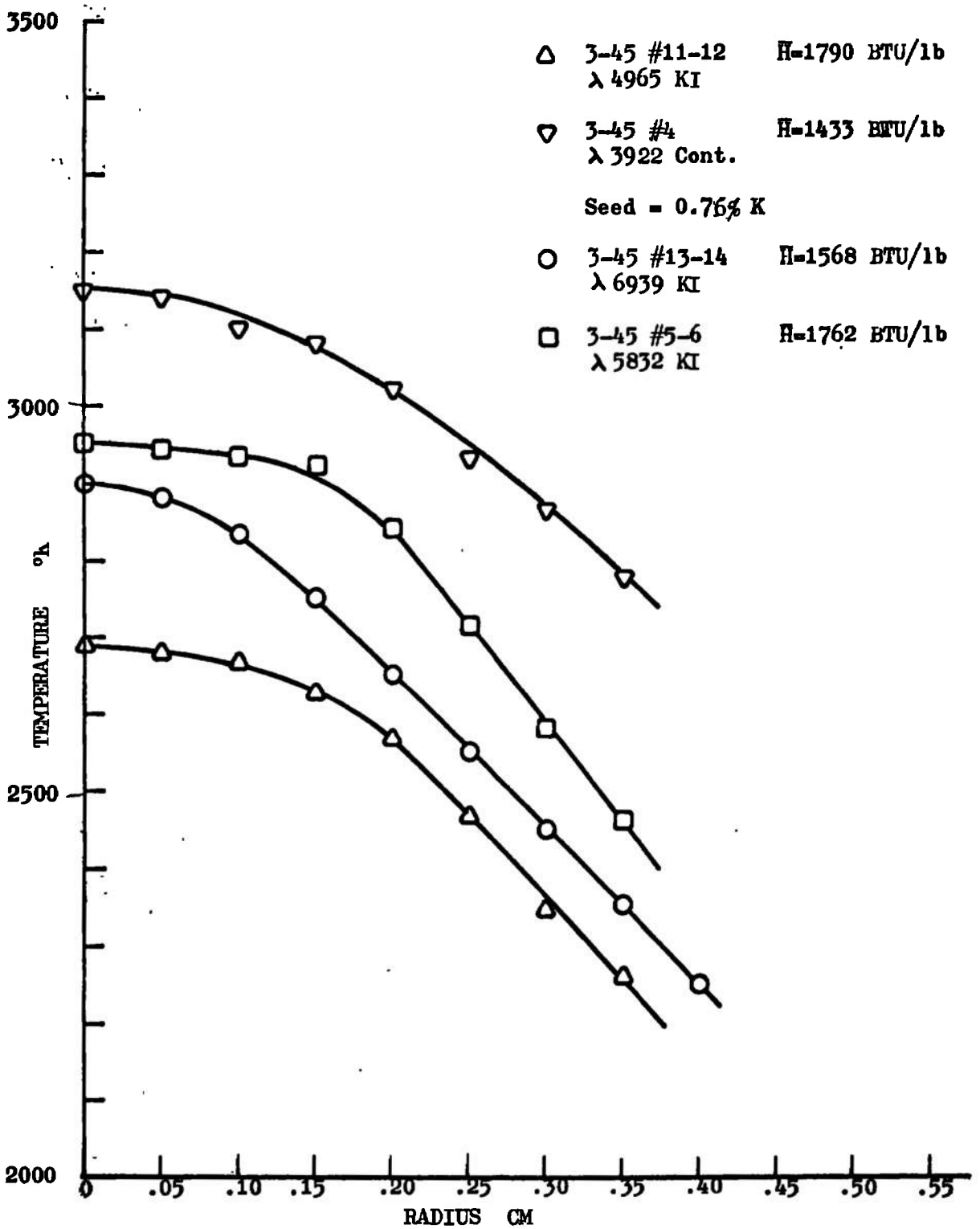

Fig. 27. Radial temperature profiles of the 1 atm 0.76% seeded air plasma obtained from absolute emission coefficients of four species of radiation.

Table I. Operating characteristics and average internal properties of seeded and unseeded experimental plasma jets.

IDENTIFICATION	FEED GAS lb/hr				SEED	JET	V	I	H_{ave} (static)	T_{ave}	T_{meas}	POSITION
Trace #	Primary	Window	Fluidizing	Carrier	% by Wt.	Config	(volts)	(amp)	(BTU/lb)	°K	°K	Inch
3-5-1	N_2 6.52	0	0	0	0	1	220	91	5180	6010	-	-
3-5-3	N_2 5.43	0	0	0	0	1	200	110	6300	6300	-	-
3-7-1	N_2 6.91	0	0	0	0	2	220	100	5740	6110	-	-
3-7-4	N_2 8.30	0	0	0	0	2	225	90	4480	5810	-	-
3-8-21	N_2 5.83	0	0	0	0	2	208	145	8336	6650	-	-
3-18-1	N_2 6.98	0	0	0	0	2	223	100	4579	5850	-	-
3-18-2	N_2 6.98	0	0	O_2 1.34	0	2	220	100	3763	5520	-	-
3-19-6	N_2 6.68	0	0	0	0	2	200	100	4423	5800	-	0.1
3-19-7	N_2 6.68	0	0	N_2 4.84	0	2	190	100	1797	3430	-	0.1
3-21-12 → 17	N_2 6.68	0	0	0	0	2	200	100	5135	6000	10,000	0.1
3-22-16	N_2 6.68	0	0	N_2 1.90	0	2	195	100	3007	5050	6,500	0.2
3-22-18 & 19	N_2 6.68	0	0	N_2 1.90	1.8	2	185	100	2609	4680	5,200	0.2
3-24-12	N_2 6.73	0	0	N_2 1.94	0	2	193	100	3300	5280	-	0.2
3-24-14 & 16	N_2 6.73	0	0	N_2 1.94	0	2	188	100	3100	3130	-	0.2
3-24-17	N_2 6.73	0	0	N_2 1.94	0	2	186	100	2950	5000	-	0.2
3-24-18 → 23	N_2 6.73	0	0	N_2 1.94	0	2	184	110	3244	5230	-	0.2
3-26-1 → 3	N_2 6.73	0	0	N_2 1.94	0	2	168	110	2575	4650	-	0.2
3-26-4 → 8	N_2 6.73	0	0	N_2 1.94	0	2	171	110	2704	4780	-	0.2
3-26-9 & 10	N_2 6.73	0	0	N_2 1.94	0	2	168	110	2575	4650	-	0.2
3-26-11 → 13	N_2 6.73	0	0	N_2 1.94	0	2	170	110	2661	4730	-	0.2
3-26-14 & 15	N_2 6.73	0	0	N_2 1.94	0	2	170	100	2540	4590	-	0.2
3-26-16 → 18	N_2 6.73	0	0	N_2 1.94	0	2	175	100	2737	4770	-	0.2
3-26-19 → 23	N_2 6.73	0	0	N_2 1.94	0	2	173	100	2658	4730	-	0.2

Table I. (cont)

IDENTIFICATION	FEED GAS lb/hr				SEED	JET	V	I	H_{ave} (static)	T_{ave}	T_{meas}	POSITION
Trace #	Primary	Window	Fluidizing	Carrier	%by Wt.	Config	(volts)	(amp)	(BTU/lb)	°K	°K	Inch
3-26-24 & 25	N_2 6.73	0	0	N_2 1.94	0	2	168	115	3454	5380	-	0.2
3-26-26	N_2 6.73	0	0	0	0	2	168	115	4482	5810	-	0.2
3-28-16→21	N_2 6.73	0	0	N_2 1.94	0	2	170	100	2255	4180	-	0.2
3-31-1 & 2	N_2 7.12	0	N_2 5.58	N_2 2.17	0	2	160	100	1650	3180	-	0.2
3-35-16→19	N_2 7.10	N_2 4.35	N_2 0.70	N_2 5.50	0	2	171	100	4100	5680	-	0.3
3-35-20→26	N_2 7.10	N_2 4.35	N_2 0.70	N_2 5.50	0.9	2	161	100	2158	4020	-	0.3
3-37-1→4	N_2 6.62	N_2 4.35	N_2 0.85	N_2 4.82	1.0	3	157	100	2400	4400	-	0.3
3-37-5→10	N_2 6.62	N_2 4.35	N_2 0.85	N_2 4.82	1.0	3	163	100	2400	4400	-	0.3
3-37-11 & 12	N_2 6.62	N_2 4.35	N_2 0.85	N_2 4.82	1.5	3	163	100	2400	4400	-	0.3
3-37-13→16	N_2 6.62	N_2 4.35	N_2 0.85	N_2 4.82	2.0	3	163	100	2400	4400	-	0.3
3-40-1→17	N_2 6.62	N_2 5.20	N_2 0.85	N_2 4.82	1.0	3	160	100	2238	4140	-	0.3
3-41-1→6	N_2 6.03	N_2 5.20	AIR 5.03	O_2 1.70	0.46	3	172	100	2330	3450	-	0.3
3-41-7→9	N_2 6.03	N_2 5.20	AIR 5.03	O_2 1.70	0.46	3	148	100	1868	3000	-	0.3
3-42-1→13	N_2 6.03	N_2 5.20	AIR 5.03	O_2 1.70	0.80	3	158	100	1990	3125	-	0.3
3-43-1→6	N_2 6.03	N_2 4.35	AIR 5.03	O_2 1.70	0.88	3	156	100	1908	3050	3150	0.3
3-43-7→10	N_2 6.03	N_2 4.35	AIR 5.03	O_2 1.70	0.88	3	145	100	1775	2900	3150	0.3
3-44-1→7	N_2 6.03	N_2 4.33	N_2 4.74	N_2 1.44	0	3	163	100	1812	3410	2900	0.3
3-44-8→21	N_2 6.03	N_2 4.33	N_2 4.74	N_2 1.44	0.94	3	163	100	1812	3410	2900	0.3
3-45-1 & 2	N_2 6.00	N_2 3.89	AIR 4.93	0	0	3	163	100	1777	2900	2900	0.3
3-45-3→14	N_2 6.00	N_2 3.89	AIR 4.93	O_2 1.69	0.76	3	163	100	1777	2900	2900	0.3
3-46-1→5	N_2 6.00	N_2 4.33	N_2 4.84	0	0	3	183	100	2040	3840	3100	0.3
3-46-6→16	N_2 6.00	N_2 4.33	N_2 4.84	N_2 1.48	0.71	3	172	100	2200	4100	3100	0.3

Table I. (cont)

IDENTIFICATION	FEED GAS lb/hr				SEED	JET	V	I	H_{ave} (static)	T_{ave}	T_{meas}	POSITION
Trace #	Primary	Window	Fluidizing	Carrier	%by Wt.	Config	(volts)	(amp)	(BTU/lb)	°K	°K	Inch
3-47-1 → 5	N_2 6.00	N_2 3.46	N_2 1.21	0	0	3	188	100	3020	5070	-	0.3
3-47-6 → 10	N_2 6.00	N_2 3.46	N_2 1.21	N_2 1.48	0.47	3	179	100	2659	4720	3000	0.3
3-47-11 → 16	N_2 6.00	N_2 3.46	N_2 1.21	N_2 1.48	0.47	3	178	100	2976	5050	3000	0.3
3-48-1 → 6	N_2 4.43	N_2 3.46	N_2 2.12	0	0	3	234	98	5932	6120	-	0.3
3-48-7 → 17	N_2 3.28	N_2 3.46	N_2 2.12	N_2 1.06	0.84	3	216	100	3020	5070	3250	0.3
3-49-1 & 2	N_2 3.28	N_2 3.46	AIR 2.12	O_2 0.92	1.20	3	215	100	2592	3650	-	0.3
3-49-3	N_2 3.28	N_2 3.46	AIR 2.12	O_2 0.92	1.20	3	208	100	2538	3670	3300	0.3
3-49-4	N_2 3.28	N_2 3.46	AIR 2.12	O_2 0.92	1.20	3	205	100	2484	3560	3300	0.3
3-49-5 & 6	N_2 3.28	N_2 3.46	AIR 2.12	O_2 0.92	1.20	3	204	100	2916	3920	3300	0.3
3-49-7 → 14	N_2 3.28	N_2 3.46	AIR 2.12	O_2 0.92	1.20	3	205	100	2800	3850	2850	0.3
3-51-3 → 6	N_2 5.10	0	0	0	0	1	205	140	4480	5800		0.12
3-52-1 → 11	N_2 5.10	0	0	0	0	1	206	140	5520	6080		0.07

Table II. Partition functions of species of particles included in plasma composition calculations.

T (°K)	Z_1 K	Z_2 N_2	Z_3 N	Z_4 K^+	Z_5 N_2^+	Z_6 N^+
2000	2.001	4.305^2 *	4.000	1.000	9.258^2	8.445
2500	2.003	5.942^2	4.000	1.000	1.298^3	8.553
3000	2.012	7.851^2	4.001	1.000	1.754^3	8.628
3500	2.031	1.003^3	4.004	1.000	2.310^3	8.687
4000	2.062	1.250^3	4.010	1.000	2.980^3	8.737
4500	2.110	1.525^3	4.022	1.000	3.780^3	8.755
5000	2.175	1.828^3	4.041	1.000	4.723^3	8.834
5500	2.260	2.161^3	4.069	1.000	5.821^3	8.884
6000	2.364	2.529^3	4.105	1.000	7.085^3	8.937

T (°K)	Z_7 O_2	Z_8 O	Z_9 O_2^+	Z_{10} O^+	Z_{11} NO	Z_{12} NO^+
2000	2.195^3	8.526	1.181^3	4.000	4.285^3	8.634^2
2500	3.200^3	8.617	1.908^3	4.000	6.100^3	1.193^3
3000	4.336^3	8.680	2.810^3	4.000	8.230^3	1.574^3
3500	5.810^3	8.729	3.889^3	4.000	1.071^4	2.015^3
4000	7.405^3	8.772	4.150^3	4.001	1.353^4	2.509^3
4500	9.400^3	8.813	6.600^3	4.002	1.671^4	3.064^3
5000	1.158^4	8.855	8.246^3	4.005	2.024^4	3.674^3
5500	1.419^4	8.900	1.010^4	4.009	2.416^4	4.348^3
6000	1.705^4	8.947	1.217^4	4.016	2.845^4	5.081^3

* Superscript indicates powers of 10.

Table III. Computed number densities of the 1 atm K_2CO_3 seeded nitrogen plasma.

a=0

T (°K)	K	N_2	N	K^+	N_2^+	N^+	e	b
2000	0	3.670^{18} *	3.302^{9}	0	1.426^{0}	0	1.426^{0}	0
2500	0	2.936^{18}	8.553^{11}	0	1.271^{4}	0	1.271^{4}	0
3000	0	2.447^{18}	3.396^{13}	0	5.543^{6}	4.003^{3}	5.547^{6}	0
3500	0	2.097^{18}	4.630^{14}	0	4.300^{8}	2.730^{6}	4.327^{8}	0
4000	0	1.832^{18}	3.243^{15}	0	1.124^{10}	3.618^{8}	1.160^{10}	0
4500	0	1.617^{18}	1.457^{16}	0	1.391^{11}	1.577^{10}	1.549^{11}	0
5000	0	1.420^{18}	4.772^{16}	0	9.880^{11}	3.073^{11}	1.295^{12}	0
5500	0	1.212^{18}	1.227^{17}	0	4.511^{12}	3.261^{13}	7.772^{12}	0
6000	0	9.657^{17}	2.576^{17}	0	1.426^{13}	2.166^{13}	3.592^{13}	0

a=0.001

T (°K)	K	N_2	N	K^+	N_2^+	N^+	e	b
2000	3.667^{15}	3.666^{18}	3.299^{9}	3.021^{12}	6.185^{-12}	2.164^{-19}	3.021^{12}	1.392^{-3}
2500	2.897^{15}	2.933^{18}	8.510^{11}	3.938^{13}	3.801^{-6}	1.303^{-10}	3.938^{13}	1.392^{-3}
3000	2.235^{15}	2.444^{18}	3.393^{13}	2.121^{14}	1.369^{-1}	9.894^{-5}	2.121^{14}	1.392^{-3}
3500	1.461^{15}	2.094^{18}	4.627^{14}	6.358^{14}	2.788^{1}	1.770^{0}	6.358^{14}	1.393^{-3}
4000	6.722^{14}	1.829^{18}	3.240^{15}	1.163^{15}	1.073^{3}	3.457^{3}	1.163^{15}	1.394^{-3}
4500	2.119^{14}	1.613^{18}	1.454^{16}	1.419^{15}	1.460^{7}	1.655^{6}	1.419^{15}	1.400^{-3}
5000	5.994^{13}	1.417^{18}	4.767^{16}	1.408^{15}	8.774^{8}	2.731^{8}	1.408^{15}	1.417^{-3}
5500	1.873^{13}	1.210^{18}	1.227^{17}	1.316^{15}	2.580^{10}	1.867^{10}	1.316^{15}	1.460^{-3}
6000	6.287^{12}	9.634^{17}	2.571^{17}	1.217^{15}	4.083^{11}	6.206^{11}	1.217^{15}	1.558^{-3}

* Superscript indicates powers of 10.

Table III. (cont)

a=0.005

T (°K)	K	N_2	N	K^+	N_2^+	N^+	e	b
2000	1.834^{16} *	3.651^{16}	3.293^{9}	6.756^{12}	2.754^{-12}	9.653^{-20}	6.756^{12}	6.951^{-3}
2500	1.459^{16}	2.921^{18}	8.493^{11}	8.839^{13}	1.687^{-6}	5.794^{-11}	8.839^{13}	6.951^{-3}
3000	1.175^{16}	2.434^{18}	3.386^{13}	4.863^{14}	5.948^{-2}	4.307^{-5}	4.863^{14}	6.952^{-3}
3500	8.919^{15}	2.085^{18}	4.617^{14}	1.566^{15}	1.127^{2}	7.171^{-1}	1.567^{15}	6.956^{-3}
4000	5.769^{15}	1.819^{18}	3.231^{15}	3.406^{15}	3.643^{2}	1.177^{3}	3.406^{15}	6.970^{-3}
4500	2.903^{15}	1.603^{18}	1.450^{16}	5.253^{15}	3.920^{6}	4.458^{5}	5.253^{15}	7.004^{-3}
5000	1.153^{15}	1.407^{18}	4.749^{16}	6.184^{15}	1.983^{8}	6.196^{7}	6.184^{15}	7.095^{-3}
5500	4.254^{14}	1.200^{18}	1.222^{17}	6.250^{15}	5.390^{9}	3.986^{9}	6.250^{15}	7.319^{-3}
6000	1.651^{14}	9.549^{17}	2.560^{17}	5.950^{15}	8.276^{10}	1.264^{11}	5.950^{15}	7.804^{-3}

a=0.01

T (°K)	K	N_2	N	K^+	N_2^+	N^+	e	b
2000	3.669^{16}	3.633^{18}	3.284^{9}	9.554^{12}	1.938^{-12}	6.809^{-20}	9.554^{12}	1.388^{-2}
2500	1.456^{16}	2.907^{18}	8.471^{11}	1.251^{14}	1.186^{-6}	4.083^{-11}	1.251^{14}	1.388^{-2}
3000	2.378^{16}	2.428^{18}	3.377^{13}	6.918^{14}	8.443^{-2}	3.019^{-5}	6.918^{14}	1.388^{-2}
3500	1.869^{16}	2.072^{18}	4.604^{14}	2.274^{15}	7.716^{1}	4.924^{-1}	2.274^{15}	1.389^{-2}
4000	1.320^{16}	1.808^{18}	3.222^{15}	5.152^{15}	2.394^{2}	7.757^{2}	5.152^{15}	1.393^{-2}
4500	7.735^{15}	1.592^{18}	1.444^{16}	8.578^{15}	2.384^{6}	2.721^{5}	8.578^{15}	1.401^{-2}
5000	3.667^{15}	1.395^{18}	4.729^{16}	1.101^{16}	1.104^{8}	3.464^{7}	1.101^{16}	1.422^{-2}
5500	1.487^{15}	1.188^{18}	1.216^{17}	1.183^{16}	2.821^{9}	2.059^{9}	1.183^{16}	1.467^{-2}
6000	6.279^{14}	9.446^{17}	2.546^{17}	1.160^{16}	4.198^{10}	6.445^{10}	1.160^{16}	1.564^{-2}

* Superscript indicates powers of 10.

Table IV. Computed number densities of the 1 atm K_2CO_3 seeded air plasma.

a= 0.001

T (°K)	K	K^+	e	N_2	N	N_2^+	N^+
2000	3.667^{15} *	3.021^{12}	3.021^{12}	2.891^{18}	2.929^{9}	4.876^{-12}	1.921^{-19}
2500	2.897^{15}	3.938^{13}	3.938^{13}	2.248^{18}	7.450^{11}	2.913^{-6}	1.141^{-12}
3000	2.240^{15}	2.121^{14}	2.121^{14}	1.828^{18}	2.885^{13}	1.014^{-1}	8.412^{-5}
3500	1.428^{15}	6.358^{14}	6.358^{14}	1.453^{18}	3.855^{14}	1.935^{2}	1.475^{2}
4000	6.722^{14}	1.163^{15}	1.163^{15}	1.214^{18}	2.640^{15}	7.123^{2}	1.761^{3}
4500	2.119^{14}	1.419^{15}	1.419^{15}	1.407^{18}	1.172^{16}	9.474^{6}	1.333^{6}
5000	6.006^{13}	1.408^{15}	1.411^{15}	9.351^{17}	3.872^{16}	5.820^{8}	2.222^{8}
5500	1.907^{13}	1.316^{15}	1.330^{15}	7.720^{17}	9.789^{16}	1.629^{10}	1.475^{10}
6000	7.188^{12}	1.216^{15}	1.268^{15}	6.066^{17}	2.040^{17}	2.468^{11}	4.728^{11}

T (°K)	O_2	O	O_2^+	O^+	NO	NO^+	b
2000	7.428^{17}	1.096^{15}	4.964^{-5}	3.542^{-12}	2.926^{16}	3.931^{0}	1.351^{-3}
2500	5.710^{17}	1.851^{16}	9.311^{-2}	4.632^{-5}	6.658^{16}	4.315^{4}	1.351^{-3}
3000	3.915^{17}	1.100^{17}	1.343^{1}	2.511^{0}	1.017^{17}	2.031^{7}	1.351^{-3}
3500	1.962^{17}	3.121^{17}	1.646^{6}	5.524^{3}	1.086^{17}	1.493^{9}	1.351^{-3}
4000	5.647^{16}	4.757^{17}	1.784^{7}	1.582^{6}	7.850^{16}	3.303^{10}	1.353^{-3}
4500	1.274^{16}	5.020^{17}	2.469^{8}	1.310^{9}	4.645^{16}	2.105^{11}	1.359^{-3}
5000	3.160^{15}	4.737^{17}	1.657^{9}	4.922^{9}	2.777^{16}	2.836^{12}	1.376^{-3}
5500	9.281^{14}	4.296^{17}	7.713^{9}	9.513^{10}	1.644^{16}	1.438^{13}	1.418^{-3}
6000	3.049^{14}	3.778^{17}	2.551^{11}	1.092^{12}	9.779^{15}	5.166^{13}	1.542^{-3}

* Superscript indicates powers of 10.

Table IV. (cont)

a= 0.005

T (°K)	K	K^+	e	N_2	N	N_2^+	N^+
2000	1.834^{16} *	6.756^{12}	6.756^{12}	2.867^{18}	2.918^{9}	2.163^{-12}	8.554^{-20}
2500	1.459^{16}	8.839^{13}	8.839^{13}	2.229^{18}	7.420^{11}	1.288^{-6}	5.062^{-11}
3000	1.175^{16}	4.863^{14}	4.863^{14}	1.772^{18}	2.890^{13}	4.282^{-2}	3.654^{-5}
3500	8.919^{15}	1.566^{15}	1.566^{15}	1.442^{18}	3.839^{14}	7.792^{2}	5.963^{-1}
4000	5.769^{15}	3.406^{15}	3.406^{15}	1.204^{18}	2.629^{15}	2.412^{2}	9.576^{2}
4500	2.902^{15}	5.253^{15}	5.253^{15}	1.039^{18}	1.167^{16}	2.540^{4}	3.588^{5}
5000	1.156^{15}	6.184^{15}	6.184^{15}	9.276^{17}	3.856^{16}	1.317^{8}	5.050^{7}
5500	4.255^{14}	6.250^{15}	6.250^{15}	7.658^{17}	9.759^{16}	3.440^{9}	3.127^{9}
6000	1.654^{14}	5.949^{15}	5.96^{15}	6.017^{17}	2.032^{17}	5.206^{10}	1.001^{10}

T (°K)	O_2	O	O_2^+	O^+	NO	NO^+	b
2000	7.369^{17}	1.092^{15}	7.277^{-6}	1.577^{-12}	2.903^{16}	1.744^{0}	6.749^{-3}
2500	5.664^{17}	1.843^{16}	8.601^{-1}	2.055^{-5}	6.610^{16}	1.909^{4}	6.749^{-3}
3000	3.883^{17}	1.096^{17}	1.788^{1}	1.091^{0}	1.009^{17}	8.787^{6}	6.750^{-3}
3500	1.946^{17}	3.109^{17}	2.970^{5}	2.234^{3}	1.077^{17}	6.022^{8}	6.753^{-3}
4000	5.602^{16}	4.738^{17}	6.041^{6}	5.379^{5}	7.788^{16}	1.119^{10}	6.767^{-3}
4500	1.264^{16}	5.000^{17}	6.618^{7}	3.526^{7}	4.600^{16}	9.997^{10}	6.800^{-3}
5000	3.135^{15}	4.718^{17}	3.750^{8}	1.448^{9}	2.755^{16}	6.420^{11}	6.888^{-3}
5500	9.206^{14}	4.279^{17}	1.629^{9}	2.017^{10}	1.631^{16}	3.036^{12}	7.106^{-3}
6000	3.025^{14}	3.763^{17}	5.381^{10}	2.313^{11}	9.701^{15}	1.090^{13}	7.577^{-3}

* Superscript indicates powers of 10.

Table IV. (cont)

a=0.01

T (°K)	K	K^+	e	N_2	N	N_2^+	N^+
2000	3.669^{16} *	9.555^{12}	9.555^{12}	2.839^{18}	2.903^{9}	1.514^{-12}	6.018^{-20}
2500	2.923^{16}	1.251^{14}	1.251^{14}	2.208^{18}	7.383^{11}	9.005^{-7}	3.558^{-11}
3000	2.378^{16}	6.918^{14}	6.918^{14}	1.791^{18}	2.905^{13}	2.980^{-2}	2.556^{-5}
3500	1.870^{16}	2.279^{15}	2.277^{15}	1.427^{18}	3.820^{14}	5.311^{1}	4.085^{-1}
4000	1.320^{16}	5.152^{15}	5.152^{15}	1.119^{18}	2.616^{15}	1.579^{2}	6.299^{2}
4500	7.735^{15}	8.515^{15}	8.575^{-15}	1.028^{18}	1.161^{16}	1.540^{6}	1.745^{6}
5000	3.667^{15}	1.107^{15}	1.101^{16}	9.183^{17}	3.831^{16}	7.323^{7}	2.821^{8}
5500	1.523^{15}	1.183^{16}	1.183^{16}	7.578^{17}	9.710^{16}	1.800^{9}	1.644^{10}
6000	6.281^{14}	1.160^{16}	1.161^{16}	5.957^{17}	2.022^{17}	2.646^{10}	5.116^{11}

T (°K)	O_2	O	O_2^+	O^+	NO	NO^+	b
2000	7.295^{17}	1.086^{15}	5.094^{-6}	1.110^{-12}	2.873^{16}	1.220^{0}	1.351^{-2}
2500	5.608^{17}	1.834^{16}	6.016^{-1}	1.442^{-5}	6.538^{16}	1.337^{4}	1.351^{-2}
3000	3.844^{17}	1.090^{17}	1.244^{+3}	7.630^{-1}	9.984^{16}	6.118^{6}	1.351^{-2}
3500	1.927^{17}	3.093^{17}	2.025^{5}	1.530^{+3}	1.066^{17}	4.104^{7}	1.349^{-2}
4000	5.546^{16}	4.714^{17}	3.954^{6}	1.273^{6}	7.710^{16}	7.321^{8}	1.352^{-2}
4500	1.251^{16}	4.975^{17}	4.013^{7}	5.294^{7}	4.554^{16}	6.062^{10}	1.360^{-2}
5000	3.100^{15}	4.694^{17}	2.085^{8}	1.173^{8}	2.727^{16}	3.569^{11}	1.381^{-2}
5500	9.114^{14}	4.257^{17}	8.519^{8}	1.060^{10}	1.615^{16}	1.588^{12}	1.424^{-2}
6000	2.994^{14}	3.754^{17}	2.736^{10}	1.182^{11}	9.603^{15}	5.539^{12}	1.518^{-2}

* Superscript indicates powers of 10.

Table V. Identifying parameters for doublet and triplet multiplets of the potassium atom.

POTASSIUM

Configuration		S_i	Desig.	λ_i(Å,vac)	E_m(cm^{-1})	g_m	A_T(sec^{-1})
$9^2D_{3/2}$	$4^2P_{3/2}$	4	(1)	4871.1 *	33572.11	4	3.10×10^5
$9^2D_{5/2}$	$4^2P_{3/2}$	36	(2)	4871.1 *	33572.11	6	
$9^2D_{3/2}$	$4^2P_{1/2}$	20	(3)	4857.4	33572.11	4	
$8^2D_{3/2}$	$4^2P_{3/2}$	4	(1)	4965.04 *	33178.4	4	3.90×10^5
$8^2D_{5/2}$	$4^2P_{3/2}$	36	(2)	4965.04 *	33178.4	6	
$8^2D_{3/2}$	$4^2P_{1/2}$	20	(3)	4950.82	33178.4	4	
$5^2D_{3/2}$	$4^2P_{3/2}$	4	(1)	5832.09 *	30185.7	4	3.20×10^5
$5^2D_{5/2}$	$4^2P_{3/2}$	36	(2)	5832.27 *	30185.5	6	
$5^2D_{3/2}$	$4^2P_{1/2}$	20	(3)	5812.52	30185.7	4	
$6^2S_{1/2}$	$4^2P_{3/2}$	10	(1)	6940.69 *	27450.65	2	8.95×10^6
$6^2S_{1/2}$	$4^2P_{1/2}$	5	(3)	6913.01	27450.65	2	

* Lines used in this investigation.

Table VI. Average energy levels, statistical weights and wavelengths for multiplets of the potassium atom.

	$9^2D \rightarrow 4^2P$	$8^2D \rightarrow 4^2P$	$5^2D \rightarrow 4^2P$	$6^2S \rightarrow 4^2P$
E_A	33572.11cm^{-1}	33178.36cm^{-1}	30185.69cm^{-1}	27450.65cm^{-1}
g_A	4	4	4	2
E_B	33572.11	33178.36	30185.18	——
g_B	6	6	6	——
E_c	13042.89	13042.89	13042.89	13042.89
g_c	4	4	4	4
E_D	12985.17	12985.17	12985.17	12985.17
g_D	2	2	2	2
$\bar{E}_m$	33572.11	33178.36	30185.38	27450.65
g_T	10	10	10	2
$\bar{\lambda}$ (vac)	4866.5Å	4961.6Å	5826.9Å	6931.5Å

Table VII. Computed parameters for multiplets of the potassium atom.

λ_*(Å) (vac)	$\bar{\lambda}$ (Å) (vac)	λ_3(Å) (vac)	$\bar{E}_m$(cm^{-1})	g_T	$(1+S_2/S_1)$	A_T(sec^{-1})	$f(\lambda_*, \lambda_3)/\lambda_* \bar{\lambda}$
4871.1	4866.5	4857.4	33572.1	10	10	3.10×10^5	1.4618×10^{-5}
4965.0	4961.6	4950.8	33178.4	10	10	3.90×10^5	1.3384×10^{-5}
5832.2	5826.9	5812.5	30185.4	10	10	3.20×10^5	1.1389×10^{-5}
6940.7	6931.5	6913.0	27450.7	2	—	8.95×10^6	9.5660×10^{-5}

UNCLASSIFIED

Security Classification

DOCUMENT CONTROL DATA - R & D

(Security classification of title, body of abstract and indexing annotation must be entered when the overall report is classified)

1. ORIGINATING ACTIVITY *(Corporate author)*
Plasma Sciences Laboratories, Inc.
Van Nuys, California

2a. REPORT SECURITY CLASSIFICATION
UNCLASSIFIED

2b. GROUP
N/A

3. REPORT TITLE
DEVELOPMENT OF DIAGNOSTIC METHODS FOR SEEDED AIR AND NITROGEN PLASMAS

4. DESCRIPTIVE NOTES *(Type of report and inclusive dates)*
June 15, 1967 to June 15, 1968 - Final Report

5. AUTHOR(S) *(First name, middle initial, last name)*
H. N. Olsen, G. Bedjai, F. L. Kelly, et al.

6. REPORT DATE
December 1968

7a. TOTAL NO. OF PAGES
72

7b. NO. OF REFS
7

8a. CONTRACT OR GRANT NO.
F40600-67-C-0017

b. PROJECT NO. 4344

c. Program Element 6540215F

d. Task 434412

9a. ORIGINATOR'S REPORT NUMBER(S)
AEDC-TR-68-217

9b. OTHER REPORT NO(S) *(Any other numbers that may be assigned this report)*
N/A

10. DISTRIBUTION STATEMENT
This document has been approved for public release and sale; its distribution is unlimited.

11. SUPPLEMENTARY NOTES
Available in DDC

12. SPONSORING MILITARY ACTIVITY
Arnold Engineering Development Center, Air Force Systems Command, Arnold Air Force Station, Tennessee

13. ABSTRACT
Absolute emission coefficients of nitrogen atomic lines, of a wavelength increment of the $N_2^+(1-)(0,0)$ band system, of the electron continuum and of several atomic lines of the seed material have been measured in atmospheric pressure nitrogen and air plasma jets seeded with K_2CO_3 powder. Radial temperature distributions determined from measured emission coefficients have been compared as the mean temperature of the plasma was reduced from 6000°K to 3000°K. In the lower range, which is most characteristic of the AEDC seeded air accelerator, temperatures determined from both absolute and relative intensities of atomic lines of the seed material agree well with those obtained from the electron continuum. The best species of radiation for temperature measurements in the range of 2500°K to 4000°K has, as the result of this investigation, been selected to be the continuous radiation emitted by the seed material itself. Errors in temperatures determined from the measured continuum and resulting from averaged variations in seed concentration and its uniformity of distribution are shown to be less than 5% in the lower temperature range.

DD FORM 1 NOV 65 1473

UNCLASSIFIED

Security Classification

14. KEY WORDS	LINK A ROLE	LINK A WT	LINK B ROLE	LINK B WT	LINK C ROLE	LINK C WT
potassium carbonate seed						
air						
nitrogen						
plasma jet						
diagnostics						
atmospheric pressure						
temperature measurement						
spectroscopy						
high current						
Saha equation						